J|A|C|S
ARTICLES
Published on Web 06/14/2006

Two-State Reactivity in Alkane Hydroxylation by Non-Heme Iron−Oxo Complexes

Hajime Hirao,[†] Devesh Kumar,[†] Lawrence Que, Jr.,[‡] and Sason Shaik*,[†]

Contribution from the Department of Chemistry and the Lise Meitner-Minerva Center for Computational Quantum Chemistry, The Hebrew University of Jerusalem, 91904 Jerusalem, Israel, and Department of Chemistry and Center for Metals in Biocatalysis, University of Minnesota, Minneapolis, Minnesota 55455

Received March 8, 2006; E-mail: sason@yfaat.ch.huji.ac.il

Abstract: Density functional theory is used to explore the mechanisms of alkane hydroxylation for four synthetic non-heme iron(IV)−oxo complexes with three target substrates (Kaizer, J.; Klinker, E. J.; Oh, N. Y.; Rohde; J.-U.; Song, W. J.; Stubna, A.; Kim, J.; Münck, E.; Nam, W.; Que, L., Jr. *J. Am. Chem. Soc.* **2004**, *126*, 472−473; Rohde, J.-U.; Que, L., Jr. *Angew. Chem. Int. Ed.* **2005**, *44*, 2255−2258.). The iron−oxo reagents possess triplet ground states and low-lying quintet excited states. The set of experimental and theoretical reactivity trends can be understood if the reactions proceed on the two spin states, namely two-state reactivity (TSR); an appropriate new model is presented. The TSR model makes testable predictions: (a) If crossing to the quintet state occurs, the hydroxylation will be effectively concerted; however, if the process transpires only on the triplet surface, stepwise hydroxylation will occur, and side products derived from radical intermediates would be observed (e.g., loss of stereochemistry). (b) In cases of crossing en route to the quintet transition state, one expects kinetic isotope effects (KIEs) typical of tunneling. (c) In situations where the two surfaces contribute to the rate, one expects intermediate KIEs and radical scrambling patterns that reflect the two processes. (d) Solvent effects on these reactions are expected to be very large.

1. Introduction

The role of high-valent iron−oxo complexes in oxidative transformations of C−H bonds is now commonly recognized.[1−5] Cytochrome P450 (P450) enzymes that are thought to make use of such a species are powerful oxidants capable of hydroxylating alkanes with C−H bond strengths ranging from very strong to very weak.[2,6] While still not fully characterized,[3−7] the reactive species in P450 (see Scheme 1), is considered to possess an iron−oxo moiety embedded in a porphyrin ring in a radical cationic state ([(Por$^{\bullet+}$)Fe^{IV}O]); hence, the effective oxidation state is Fe^{V}. The species is known as compound I (Cpd I, Scheme 1).[1] Many synthetic Cpd I iron-porphyrin species have been made by now and perform a great variety of oxidation processes.[2] The one-electron reduced form of Cpd I is called Cpd II (in Scheme 1) and is generally a sluggish reagent for C−H bond activation compared with Cpd I. [8,9]

Scheme 1. (a) Heme Species, Compound I (Cpd I) and Cpd II of P450, and Non-Heme $L_5Fe^{IV}O$ Complexes; (b) Some Ligands Used for Making Synthetic Non-Heme $L_5Fe^{IV}O$, and Their Name Abbreviations; (c) Hydroxylation Processes Studied between Non-Heme L_5FeO^{Z} Reagents and Organic Molecules

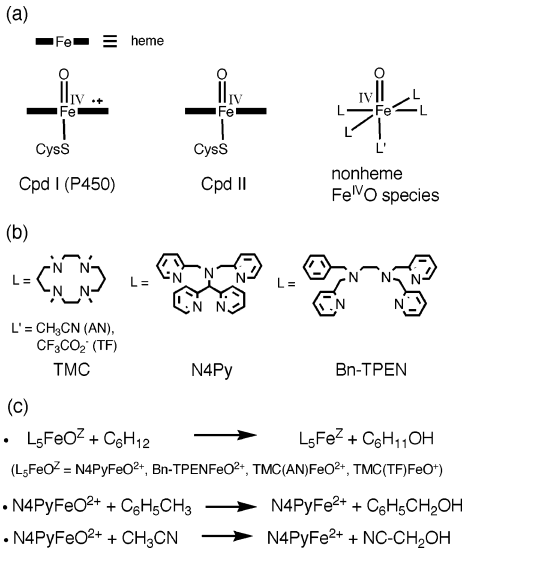

In contrast to heme systems, there exists a class of non-heme $[L_5Fe^{IV}O]^Z$ (Z = ionic charge) complexes (Scheme 1) where the species that are analogous to Cpd II are nevertheless very powerful oxidants capable of activating even strong C−H bonds, much like Cpd I of P450.[10−18] Such non-heme Fe^{IV}O species

[†] The Hebrew University of Jerusalem.
[‡] University of Minnesota.

(1) Sono, M.; Roach, M. P.; Coulter, E. D.; Dawson, J. H. *Chem. Rev.* **1996**, *96*, 2841−2888.
(2) Groves, J. T. In *Cytochrome P450: Structure, Mechanism, and Biochemistry*, 3rd ed.; Ortiz de Montellano, P. R., Ed.; Kluwer-Academic/Plenum: New York, 2005; p1.
(3) Schlichting, I.; Berendzen, J.; Chu, K.; Stock, A. M.; Maves, S. A.; Benson, D. E.; Sweet, R. M.; Ringe, D.; Petsko, G. A.; Sligar, S. G. *Science* **2000**, *287*, 1615−1622.
(4) Spolitak, T.; Dawson, J. H.; Ballou, D. P. *J. Biol. Chem.* **2005**, *280*, 20300−20309.
(5) Denisov, I. G.; Makris, T. M.; Sligar, S. G. *J. Biol. Chem.* **2001**, *276*, 11648−11652.
(6) Dowers, T. S.; Rock, D. A.; Rock, D. A.; Jones, J. P. *J. Am. Chem. Soc.* **2004**, *126*, 8868−8869.
(7) Harris, D. L. *Curr. Opin. Chem. Biol.* **2001**, *5*, 724−735.

10.1021/ja061609o CCC: $33.50

have been proposed as intermediates for iron(II) enzymes and characterized for *TauD*,[11−13] a prototypical α-ketoglutarate-dependent (α-KG) enzyme. Along with these enzymatic entities, there is a growing gallery of synthetic $L_5Fe^{IV}O^Z$ complexes that have been actually characterized by spectroscopic as well as crystallographic techniques.[14−19] Some of the ligands that were used by one of us (L.Q.) to make these species are depicted in Scheme 1b. The first isolable $L_5Fe^{IV}O^Z$ species[14] was made with the tetradentate ligand TMC, with acetonitrile (AN) as a fifth ligand; the TMC(AN)FeO^{2+} complex was crystallized and characterized by means of X-ray diffraction. This fifth ligand can undergo facile replacement and affords a variety of related complexes, including the recently synthesized TMC(TF)FeO^+ complex (TF = $CF_3CO_2^-$).[18a] Other complexes were made with the pentadentate ligands, N4Py and Bn-TPEN in Scheme 1, which by wrapping around the iron provide the needed pentacoordination about the Fe═O unit. Unlike the enzymatic species that are neutral (**Z** = 0) and have high-spin (HS) ground states with a quantum number $S = 2$,[11−13] the synthetic complexes[14−18] are cationic (**Z** = 2+, 1+) and have intermediate-spin (IS) ground states with $S = 1$. Recently, an aqueous ferryl water complex has been characterized to have an $S = 2$ ground state.[20]

The reactivity patterns of these synthetic complexes are fascinating and form the focus for the present paper. The most reactive species appear to be the N4Py−FeO^{2+} and Bn-TPEN−FeO^{2+} complexes, which hydroxylate even cyclohexane.[16] The relative reactivity of the different molecules with the two complexes showed dependence on the bond dissociation energy (D_{C-H}) of the C−H bonds undergoing activation and exhibited very large kinetic isotope effects (KIEs) when the organic molecule was deuterated.[16,17] For all the organic molecules tried so far, the Bn-TPEN−FeO^{2+} complex was found to be more reactive than N4Py−FeO^{2+}. By comparison to these two reactive complexes, the TMC(AN)−FeO^{2+} complex turned out to be inefficient for C−H activation, and at $T = 25$ °C could oxidize only 9,10-dihydroanthracene to anthracene.[18] In contrast, a change of the axial ligand of TMC(L)−FeO^{2+} from AN to TF (TMC(TF)−FeO^+) enhanced the reactivity toward the conversion of 9,10-dihydroanthracene to anthracene,[18a] and so did the TMCS−FeO^+ complex that possesses a thiolate fifth ligand.[18b] In most cases, the complexes were stable in acetonitrile, which is also the reaction medium. Since the C−H bond strength of acetonitrile (93 kcal/mol)[21] is smaller than that of C_6H_{12}, it is puzzling why the reagents do not react with CH_3CN at the rate in which they react with C_6H_{12}.

Theory can be helpful in pinpointing the factors that give rise to these intriguing trends. The importance of theory for elucidating mechanisms of oxidation by iron−oxo species was amply demonstrated in the field of P450 reactivity, where it has been shown that a dominant feature of these reactions is the two-state reactivity (TSR) that transpires due to the close proximity of the two spin states in the ground state of Cpd I of P450.[22−25] The usefulness of DFT in non-heme systems was already demonstrated by the studies of Münck, Neese, Thiel, Solomon and co-workers[18,20,26,27] who combined spectroscopic investigations and DFT studies of these iron−oxo complexes in the two possible spin states, $S = 1$ and $S = 2$. These studies led to good agreement between theory and experiment regarding the identity of the ground state as the $S = 1$ species as well as the corresponding molecular geometries, electronic structures, and the Mössbauer parameters of these complexes. Our own recent DFT investigation of the C−H hydroxylation of cyclohexane with N4Py−FeO^{2+} showed that the three different spin states ($S = 1$, 2, and 0) of the oxidant may participate in the hydroxylation process, and *the quintet state* ($S = 2$) may possibly provide a low-energy route for C−H hydroxylation if spin flip is sufficiently efficient to allow the crossover from the triplet ($S = 1$) ground state.[28] As such, it is reasonably expected that theory could be a powerful tool for tackling the reactivity problems of non-heme oxidants and, possibly, for enhancing the synergy between theory and experiment.

To apply our study of the reactivity of synthetic non-heme Fe^{IV}═O species and attempt to pattern the above reactivity puzzles, we examined here the reactivity patterns of the systems depicted in Scheme 1c. Thus, to obtain information on the relative efficacies of the oxidants, we compared the reactions of four iron−oxo complexes with cyclohexane. The persistence of the complexes in acetonitrile was probed by looking at the reaction of N4Py−FeO^{2+} with CH_3CN, while the relative reactivity of organic molecules was interrogated by looking at the reactions of N4Py−FeO^{2+} with cyclohexane and toluene. In addition, to assess the effect of the multidentate ligand on properties of the iron−oxo species, we calculated also the

(8) Groves, J. T.; Gross, Z.; Stern, M. K. *Inorg. Chem.* **1994**, *33*, 5065−5072.
(9) Nam, W.; Park, S.-E.; Lim, I. K.; Lim, M. H.; Hong, J.; Kim, J. *J. Am. Chem. Soc.* **2003**, *125*, 14674−14675.
(10) Costas, M.: Mehn, M. P.; Jensen, M. P.; Que, L., Jr. *Chem. Rev.* **2004**, *104*, 939−986.
(11) Price, J. C.; Barr, E. W.; Glass, T. E.; Krebs, C.; Bollinger, J. M., Jr. *J. Am. Chem. Soc.* **2003**, *125*, 13008−13009.
(12) Price, J. C.; Barr, E. W.; Tirupati, B.; Bollinger, J. M., Jr.; Krebs, C. *Biochemistry* **2003**, *42*, 7497−7508.
(13) Proshlyakov, D. A.; Henshaw, T. F.; Monterosso, G. R.; Ryle, M. J.; Hausinger, R. P. *J. Am. Chem. Soc.* **2004**, *126*, 1022−1023.
(14) Rohde, J.-U.; In, J.-H.; Lim, M. H.; Brennessel, W. W.; Bukowski, M. R.; Stubna, A.; Münck, E.; Nam, W.; Que, L., Jr. *Science* **2003**, *299*, 1037−1039.
(15) Rohde, J.-U.; Torelli, S.; Shan, X.; Lim, M. H..; Klinker, E. J.; Kaizer, J.; Chen, K.; Nam, W.; Que, L., Jr. *J. Am. Chem. Soc.* **2004**, *126*, 16750−16761.
(16) Kaizer, J.; Klinker, E. J.; Oh, N. Y.; Rohde; J.-U.; Song, W. J.; Stubna, A.; Kim, J.; Münck, E.; Nam, W.; Que, L., Jr. *J. Am. Chem. Soc.* **2004**, *126*, 472−473.
(17) Oh, N. Y.; Suh, Y.; Park, M. J.; Seo, M. S.; Kim, J.; Nam, W. *Angew. Chem., Int. Ed.* **2005**, *44*, 4235−4239.
(18) (a) Rohde, J.-U.; Que, L., Jr. *Angew. Chem., Int. Ed.* **2005**, *44*, 2255−2258. (b) Bukowski, M. R.; Koehntop, K. D.; Stubna, A.; Bominaar, E. L.; Halfen, J. A.; Münck, E.; Nam, W.; Que, L., Jr. *Science* **2005**, *310*, 1000−1002.
(19) Other L_5FeO complexes: (a) MacBeth, C. E.; Golombek, A. P.; Young, V. G., Jr.; Yang, C.; Kuczera, K.; Hendrich, M. P.; Borovik, A. S. *Science* **2000**, 289, 938−941. (b) MacBeth, C. E.; Gupta, R.; Mitchell-Koch, K. R.; Young, V. G., Jr.; Lushington, G. H.; Thompson, W. H.; Hendrich, M. P.; Borovik, A. S. *J. Am. Chem. Soc.* **2004**, *126*, 2556−2567. (c) Grapperhaus, C. A.; Mienert, B.; Bill, E.; Weyhermüller, T.; Wieghardt, K. *Inorg. Chem.* **2000**, *39*, 5306−5317. (d) Berry, J. F.; Bill, E.; Bothe, E.; Weyhermüller, T.; Wieghardt, K. *J. Am. Chem. Soc.* **2005**, *127*, 11550−11551.
(20) Pestovsky, O.; Stoian, S.; Bominaar, E. L.; Shan, X.; Münck, E.; Que, L., Jr.; Bakac, A. *Angew. Chem., Int. Ed.* **2005**, *44*, 6871−6874.
(21) (a) McMillen, D. F.; Golden, D. M. *Annu. Rev. Phys. Chem.* **1982**, *33*, 483−532. (b) Bordwell, F. G.; Harrelson, J. A., Jr.; Zhang, X. *J. Org. Chem.* **1991**, *56*, 4448−4450.
(22) Ogliaro, F.; Harris, N.; Cohen, S.; Filatov, M.; de Visser, S. P.; Shaik, S. *J. Am. Chem. Soc.* **2000**, *122*, 8977−8989.
(23) de Visser, S. P.; Ogliaro, F.; Sharma, P. K.; Shaik, S. *J. Am. Chem. Soc.* **2002**, *124*, 11809−11826.
(24) Kumar, D.; de Visser, S. P.; Sharma, P. K.; Cohen, S.; Shaik, S. *J. Am. Chem. Soc.* **2004**, *126*, 1907−1920.
(25) Hirao, H.; Kumar, D.; Thiel, W.; Shaik, S. *J. Am. Chem. Soc.* **2005**, *127*, 13007−13018.
(26) (a) Decker, A.; Rohde, J.-U.; Que, L., Jr.; Solomon, E. I. *J. Am. Chem. Soc.* **2004**, *126*, 5378−5379. (b) Decker, A.; Solomon, E. I. *Angew. Chem., Int. Ed.* **2005**, *44*, 2252−2255.
(27) See: Schöneboom, J. C.; Neese, F.; Thiel, W. *J. Am. Chem. Soc.* **2005**, *127*, 5840−5853.
(28) Kumar, D.; Hirao, H.; Que, L., Jr.; Shaik, S. *J. Am. Chem. Soc.* **2005**, *127*, 8026−8027.

pristine $(NH_3)_5FeO^{2+}$ complex and the TMC−FeO^{2+} complex devoid of the fifth ligand. As simple notations for the iron−oxo reagents, we shall use throughout the symbol[28] $^{2S+1}\mathbf{K}_{\mathbf{L}}^{\mathbf{Z}}$, where the L indicates the ligand, L = N4Py, Bn-TPEN, TMC, TMC(AN), or TMC(TF), where TMC is the tetracoordinate macrocyclic ligand devoid of a fifth axial ligand, while AN and TF signify the fifth ligand, CH_3CN and $CF_3CO_2^-$. The left-hand superscript $2S+1$ indicates the spin state; the study involved $S = 1$, 2, and 0. The superscript, Z indicates the molecular charge.

2. Computational Details

The study generated many computational results that are collected in the Supporting Information (SI). The key data are discussed in the text.

Standard Methods. All the geometries were optimized with Jaguar 5.5[29] at the UB3LYP/LACVP level (UB3LYP/B1).[30,31] Reaction pathways were verified by scan calculations along a given internuclear distance, while optimizing freely the positions of all other atoms. The geometry at the top of the energy scan was used for subsequent optimization of a transition state. Frequency calculations were performed for all species using Gaussian 03.[32] Single-point calculations on the LACVP-optimized geometry were subsequently carried out with the larger LACV3P++** basis set (B2).[31] The solvent effect was also calculated with B2 using acetonitrile as a solvent ($\epsilon = 37.5$, probe radius = 2.183 Å). To evaluate the effect of zero-point energy (ZPE) correction, the frequencies were scaled by the factor, 0.9806.[33] Since the scaling did not affect relative energies much (~0.1 kcal/mol), we report unscaled ZPE values throughout.

Tests of the OPBE Functional. UB3LYP gives generally good results for these non-heme systems and predicts properly the identity of the ground state as the triplet state, with $S = 1$.[18,20,26a,27,34,35] Nevertheless, to ascertain the choice of UB3LYP, we used also the OPBE pure (GGA) exchange functional [36] that was tested successfully on spin-state ordering of iron complexes.[37] The results on the various spin states of $\mathbf{K}_{\mathbf{TMC(AN)}}$ and $\mathbf{K}_{\mathbf{TMC(TF)}}$ (see Table S11 in the SI) showed that the triplet−quintet gaps are smaller than those predicted by UB3LYP. For $\mathbf{K}_{\mathbf{TMC(TF)}}$, the UOPBE/B2//UB3LYP/B1 calculations predicted a quintet ground state, whereas experiment assigns this species as a triplet $S = 1$ ground state.[18a] An additional test with UOPBE was performed on the relative energy of the transition states for the reaction of the N4Py with cyclohexane (**CH**) (see Scheme 1c). The results (see Table S12 for UOPBE/B2//UB3LYP/B1 data) predicted spin-state crossing much like UB3LYP. Since the UB3LYP calculations led to the correct spin ordering for all the $^{2S+1}\mathbf{K}_{\mathbf{L}}^{\mathbf{Z}}$ reagents, and for others as well,[20] we selected UB3LYP as the choice method. The accuracy of UB3LYP for this kind of systems is documented in the SI.

Locating the Seam of Spin-State Crossing. To get some information on the mechanism of spin-state crossing, we calculated the seam of triplet−quintet crossing along the hydroxylation pathways, using the program of Harvey and Aschi that is adaptable to DFT calculations.[38] Since these calculations are time-consuming, they were limited to the B1 basis set and hence only to the reactions where the state crossing occurs at the UB3LYP/B1 level.

Scheme 2. Electronic Configurations in the d-Block Orbitals of the Lowest Spin-States of $^{2S+1}\mathbf{K}_{\mathbf{L}}^{\mathbf{Z}}$ Complexes; Orbital Drawings Were Made with *MOLEKEL*[39]

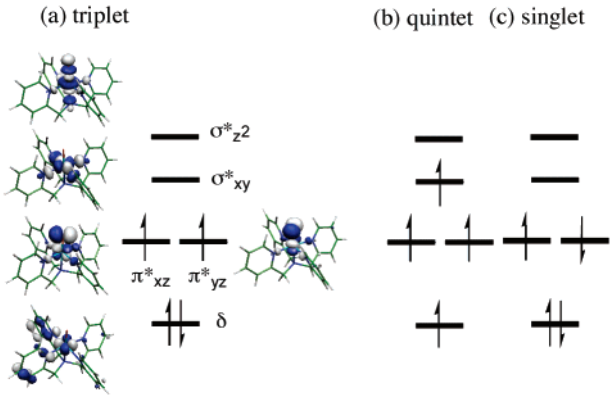

3. Results and Discussion

3.1. Properties of the Iron−Oxo Complexes, $^{2S+1}\mathbf{K}_{\mathbf{L}}^{\mathbf{Z}}$. The electron occupancies in the d-block orbitals of the three lowest spin states of the $^{2S+1}\mathbf{K}_{\mathbf{L}}^{\mathbf{Z}}$ species are depicted in Scheme 2. The scheme shows a triplet state with a $\delta^2\pi^*_{xz}{}^1\pi^*_{yz}{}^1$ configuration, a corresponding open-shell singlet $\delta^2\pi^*_{xz}{}^1\pi^*_{yz}{}^1$ state, and a quintet $\delta^1\pi^*_{xz}{}^1\pi^*_{yz}{}^1\sigma^*_{xy}{}^1$ state. This section summarizes some computed properties of these species.

Spin-State Ordering of the Iron−Oxo Complexes, $^{2S+1}\mathbf{K}_{\mathbf{L}}^{\mathbf{Z}}$. Figure 1 shows key bond lengths in the UB3LYP/B1 optimized geometries of the three spin states for all the $\mathbf{K}_{\mathbf{L}}^{\mathbf{Z}}$ reagents, as well as the corresponding energies relative to the triplet state at various levels. In part (a) of the figure we show the lowest two states, triplet and quintet, while in part (b) of the figure we show the data for the singlet state. The relative energy (E_{rel}) data are arranged in two lines; in the first line we display B1//B1 values followed by ZPE corrected values in parentheses, and in the second line we show B2//B1 values, followed by ZPE corrected values in parentheses and with solvation correction added in the square bracket.

Inspection of Figure 1 shows that, at the UB3LYP/B1//B1 level, the triplet state is the ground state and is favored by >5 kcal/mol over the quintet state. Adding ZPE correction shrinks this gap, and a single-point calculation at the UB3LYP/B2//B1 level further reduces it. At the highest level, B2//B1 with ZPE and solvation corrections, all the species possess triplet ground states in accord with experiment.[14,15] Another good feature of the results is that, despite the quantitative changes, the trends remain approximately the same, namely the gaps decrease in the order of L = TMC > N4Py ≈ 5(NH_3) > Bn-TPEN ≈ TMC-(AN) > TMC(TF). The UB3LYP energy gap results for the series[18a,27,40,41] are in accord with experiment, and in the case

(29) *Jaguar 5.5*; Schrödinger, Inc.: Portland, Oregon, 2004.
(30) (a) Becke, A. D. *J. Chem. Phys.* **1992**, *96*, 2155−2160. (b) Becke, A. D. *J. Chem. Phys.* **1992**, *97*, 9173−9177. (c) Becke, A. D. *J. Chem. Phys.* **1993**, *98*, 5648−5652. (d) Lee, C.; Yang, W.; Parr, R. G. *Phys. Rev. B* **1988**, *37*, 785−789.
(31) The LACVP series is derived from LANL2DZ, see: (a) Hay, J. P.; Wadt, W. R. *J. Chem. Phys.* **1985**, *82*, 299−310. (b) Friesner, R. A.; Murphy, R. B.; Beachy, M. D.; Ringnalda, M. N.; Pollard, W. T.; Dunietz, B. D.; Cao, Y. *J. Phys. Chem. A* **1999**, *103*, 1913−1928.
(32) Frisch, M. J.; et al. *Gaussian 03*, Revision C.02. Gaussian, Inc.: Wallingford, CT, 2004.
(33) Scott, A. P.; Radom, L. *J. Phys. Chem.* **1996**, *100*, 16502−16513.
(34) Bassan, A.; Blomberg, M. R. A.; Siegbahn, P. E. M. *Chem. Eur. J.* **2003**, *9*, 4055−4067.
(35) Quiñonero, D.; Morokuma, K.; Musaev, D. G.; Mas-Ballesté, R.; Que, L., Jr. *J. Am. Chem. Soc.* **2005**, *127*, 6548−6549.
(36) (a) Handy, N. C.; Cohen, A. *Mol. Phys.* **2001**, *99*, 403−412. (b) Perdew, J. P.; Burke, K.; Ernzerhof, M. *Phys. Rev. Lett.* **1996**, *77*, 3865−3868.
(37) (a) Swart, M.; Ehlers, A. W.; Lammertsma, K. *Mol. Phys.* **2004**, *102*, 2467−2474. (b) Groenhof, A. R.; Swart, M.; Ehlers, A. W.; Lammertsma, K. *J. Phys. Chem. A* **2005**, *109*, 3411−3417.
(38) Harvey, J. N.; Aschi, M.; Schwarz, H.; Koch, W. *Theor. Chem. Acc.* **1998**, *99*, 95−99.
(39) (a) Flükiger, P.; Lüthi, H. P.; Portmann, S.; Weber, J. *MOLEKEL 4.2*; Swiss Center for Scientific Computing: Manno, Switzerland, 2000−2002. (b) Portmann, S.; Lüthi, H. P. *CHIMIA* **2000**, *54*, 766−770.
(40) For a comparison of UB3LYP and SORCI and DCCI calculations of Cpd I and $\mathbf{K}_{\mathbf{TMC(AN)}}$, see ref 27 above.

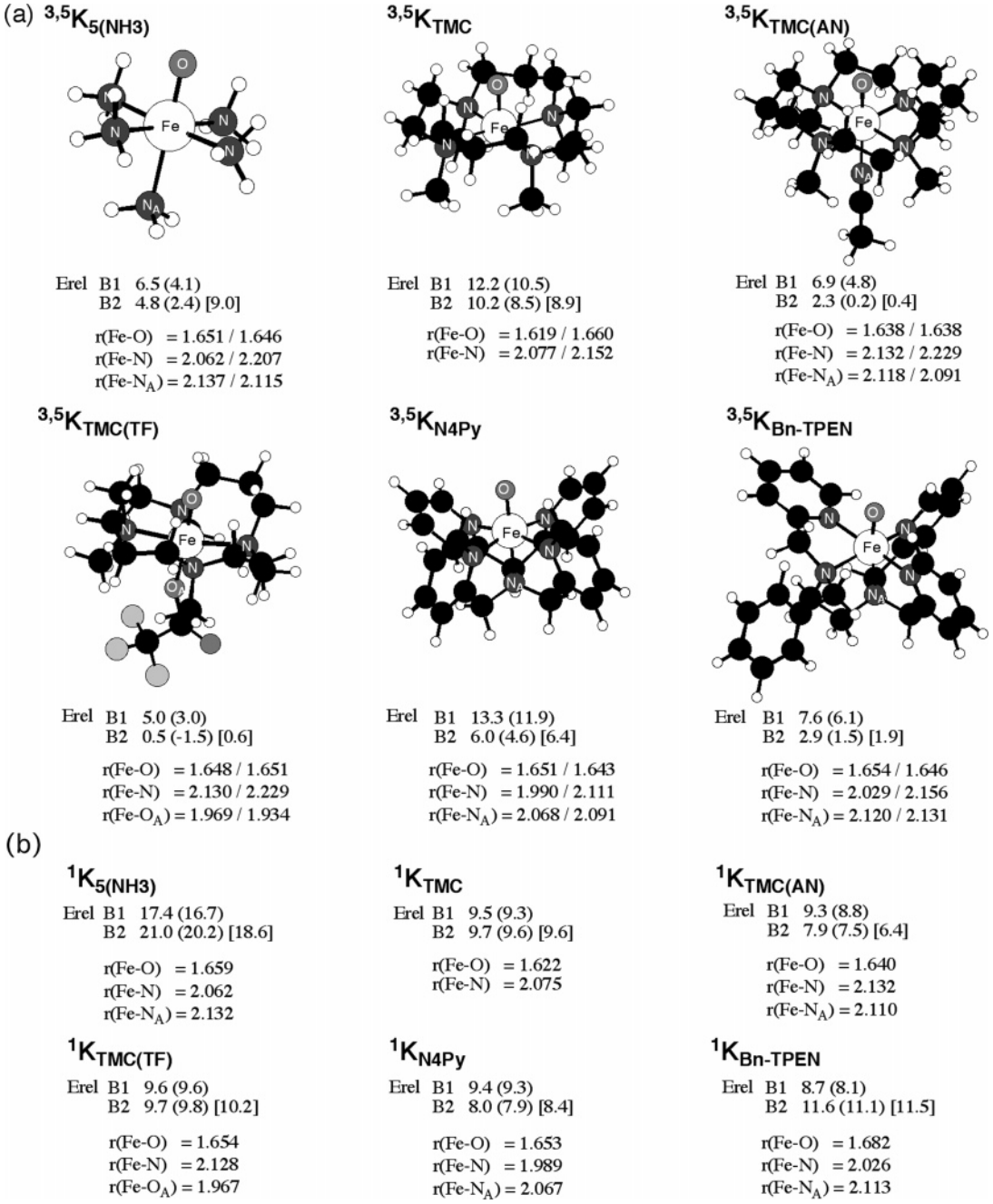

Figure 1. (a) B1 optimized structures and relative energies (in kcal/mol) of $^{3,5}\mathbf{K_L}^{\mathbf{Z}}$ species. The triplet state is defined as the zero of the energy. The relative energy values correspond to: energy (energy + ZPE correction) [energy + ZPE + solvation corrections]. Key bond lengths are shown for triplet/quintet states, respectively. (b) Corresponding data for the $^{1}\mathbf{K_L}^{\mathbf{Z}}$ state.

ofTMC(AN) it is also in accord with high level ab initio calculations.[27]

Discussion of the Trends in Spin-State Ordering of $^{3}\mathbf{K_L}^{\mathbf{Z}}$ (Z = 1, 2) Complexes. The state ordering, in Figure 1, is determined by a combination of a few factors: (i) the $\delta-\sigma^*_{xy}$ orbital energy gap (Scheme 2), (ii) the exchange interactions among the unpaired electrons in the d-block, and (iii) the energy changes due to geometric differences. The exchange energy[42] would prefer the quintet state, while the orbital energy gap and the geometric variations favor the triplet state. The orbital energy gap depends on the binding strength of the equatorial Fe−N bonds as well as on the electron−electron repulsion between the electrons of axial ligand and the electron pair in the δ orbital in the triplet state and the extent of long-range antibonding Fe−N interaction in the δ orbital (See Scheme 2). The stronger the Fe−N_{eq} binding, the higher the corresponding σ^*_{xy} orbital is, and the larger the gaps are. The stronger the electron−electron repulsion of the axial ligand with the electron pair in δ orbital of Fe, the easier it would be to excite an electron to the σ^*_{xy} orbital and stabilize the quintet state. Thus, among the hexacoordinated experimental complexes, the ligand N4Py makes the shortest Fe−N_{eq} bonds and possesses the largest energy gap. The electron−electron repulsion with the axial ligand is apparent from the series TMC, TMC(AN) and TMC-

(41) Krebs, C.; Price, J. C.; Baldwin, J.; Saleh, L.; Green, M. T.; Bollinger, J. M., Jr. *Inorg. Chem.* **2005**, *44*, 742−757.
(42) Carter, E. A.; Goddard, W. A., III. *J. Phys. Chem.* **1988**, *92*, 5679−5683.

Table 1. Comparison of UB3LYP/B1 Optimized Geometrical Values with Experimental Data (in Parentheses) for Triplet Iron−Oxo Species, $^3\mathbf{K}_L$ (in Å)

	r(Fe–O)	*r*(Fe–N) [a]	*r*(Fe–N_A) or *r*(Fe–O_A)
$^3\mathbf{K}_{5(NH3)}$	1.651 (NA)	2.062 (NA)	2.137 (NA)
$^3\mathbf{K}_{N4Py}$ [b]	1.651 (1.65)	1.990 (1.97)	2.068 (2.12)
$^3\mathbf{K}_{TMC}$	1.619 (NA)	2.077 (NA)	− (−)
$^3\mathbf{K}_{TMC(AN)}$ [c]	1.638 (1.646)	2.132 (2.091)	2.118 (2.058)
$^3\mathbf{K}_{TMC(TF)}$	1.648 (NA)	2.130 (NA)	1.969 (NA)
$^3\mathbf{K}_{Bn-TPEN}$ [b]	1.654 (1.67)	2.029 (2.00)	2.120 (2.18) [d]

[a] Averaged value of four Fe−N distances. [b] Reference 15. [c] Reference 14. [d] From the 10th fitting (see ref 15).

(TF); the first case being devoid of an axial ligand has the largest gap, while the last case, where the axial ligand possesses a negative charge, has the smallest gap. This is likey also the reason N4Py has a smaller gap compared with the pentacoordinate $\mathbf{K_{TMC}}$ complex. Thus, the relative energy of the two lowest electronic states is a fine balance between a few factors, and this balance may be very sensitive to the level and type of calculations. It is gratifying, though, that the trends are similar at the various levels, which shows that the quintet−triplet-state gaps decrease in the order of L = TMC > N4Py ≈ 5(NH_3) > Bn-TPEN ≈ TMC(AN) > TMC(TF).

Geometric Features of the Iron−Oxo Complexes, $^{2S+1}\mathbf{K}_L^Z$. The geometric data of the species in Figure 1 reveal, in accord with previous conclusions,[20,26b,27,41] a fairly constant Fe=O bond length. By contrast, the Fe−N_{eq} bonds undergo lengthening in the quintet state, in accord with the occupation of the σ^*_{xy} orbital in this state (Scheme 2). The Fe−L_{ax} distances to the axial ligand undergo very slight changes, and for the TMC(AN) and TMC(TF) ligands, the bonds are even slightly shortened; this shortening may reflect reduced steric repulsion with the TMC ligand or reduced electron repulsion with the iron due to the excitation of the electron from the δ orbital that is located on the iron to the more diffuse σ^*_{xy} orbital. Table 1 collects the critical bond lengths for all the iron−oxo species in the triplet ground state and wherever possible compares them to experiment. It is seen that the computed data is in reasonable accord with experiment.

Electron Affinities of the $^3\mathbf{K}_L^Z$ (Z = 1, 2) Complexes. Since oxidation may occur by initial single-electron transfer from the organic molecule to the iron−oxo complex, we calculated the corresponding electron affinities (ionization energies of the $^4\mathbf{K}_L^{Z-1}$ species with an excess electron in the σ^*_{xy} orbital) in the gas phase and in solution. The data are summarized in Table 2. It is seen that the ionization energies of the $^4\mathbf{K}_L^{Z-1}$ species with the excess electron are very large in the gas phase; it is largest for the $^4\mathbf{K}_{5(NH3)}^{1+}$ complex, reflecting the lesser electron repulsion, with the excess electron, exerted by the smaller ligands compared with the larger ones. For the experimental complexes the ionization energy is the largest for $^4\mathbf{K}_{TMC}^{1+}$ and smallest for $^4\mathbf{K}_{TMC(TF)}^{0}$, reflecting in the latter the electron repulsion with the negatively charged ligand. The solvent exerts a great leveling effect and makes $^3\mathbf{K}_{Bn-TPEN}$ the strongest electron acceptor, while $^3\mathbf{K}_{TMC(TF)}$ remains the weakest. This leveling effect is expected since the solvent stabilizes the $^4\mathbf{K}_L^{Z-1}$ species less than the $^3\mathbf{K}_L^Z$ complexes, due to the higher positive charge of the latter species.

To test the possibility of an electron-transfer reaction during oxidation of 9,10-dihydroanthracene, we calculated also the ionization potential of the organic molecule in the gas phase and in solution. As can be seen from the data in Table 2, an electron transfer would be highly endothermic. As such, a mechanism with an initial electron-transfer step is ruled out as the source of reactivity of $^3\mathbf{K}_{TMC(AN)}$ and $^3\mathbf{K}_{TMC(TF)}$ toward 9,10-dihydroanthracene.

Table 2. UB3LYP/B1 Calculated Electron Affinities[a] of ^3K_L Complexes (in kcal/mol)

	gas phase		solution (ϵ=37.5)	
species	EA_v [b]	EA_{ad} [b]	EA_v [b]	EA_{ad} [b]
$^3\mathbf{K}_{5(NH3)}$	210.6	229.3	75.8	84.9
$^3\mathbf{K}_{N4Py}$	167.8	182.8	77.3	93.4
$^3\mathbf{K}_{TMC}$	195.2	207.7	87.0	98.3
$^3\mathbf{K}_{TMC(AN)}$	187.4	197.8	86.7	95.1
$^3\mathbf{K}_{TMC(TF)}$	117.5	129.1	79.6	90.5
$^3\mathbf{K}_{Bn-TPEN}$	173.2	188.1	84.9	100.4
	IP_v [b]	IP_{ad} [b]	IP_v [b]	IP_{ad} [b]
dihydroanthracene	183.5	179.5	142.8	138.2

[a] Calculated as the ionization energies of the anion: $^4\mathbf{K}_L^{Z-1} \rightarrow {}^3\mathbf{K}_L^Z + e^-$. The excess electron in $^4\mathbf{K}_L^{Z-1}$ occupies the σ^*_{xy} orbital. [b] The subscript "v" means vertical, i.e., both species share the same geometry as that for $^3\mathbf{K}_L^Z$. The subscript "ad" means "adiabatic" and refers to a process where both species have relaxed geometries in the gas phase.

Table 3. UB3LYP/B1 Calculated Bond Dissociation Energies (D_{Fe-Lax}) in $^3\mathbf{K}_{TMC(Lax)}$ Complexes (in kcal/mol)[a]

D_{Fe-Lax} quantity	D_{Fe-AN}	D_{Fe-TF}
ΔE	29.9	193.4
$\Delta(E+E_{solv})$	13.2	25.1
$\Delta(E+ZPE+E_{solv})$	10.8	22.0

[a] These quantities refer to the process; $^3\mathbf{K}_{TMC(Lax)} \rightarrow {}^3\mathbf{K}_{TMC} + \mathbf{L}_{ax}$.

Bond Energies of the Axial Ligands in the $^3\mathbf{K}_{TMC(AN)}$ and $^3\mathbf{K}_{TMC(TF)}$. Since the axial ligand plays a role in the reactivity of the TMC(L_{ax})−FeO complexes,[18] it was deemed essential to ascertain that the axial ligand remains intact during the reactions. Table 3 shows the bond dissociation energies for the axial ligand (L_{ax}), D_{Fe-Lax}, calculated at the UB3LYP/B1 level. It is seen that in the gas-phase the D_{Fe-Lax} values are large, especially for the $CF_3CO_2^-$ ligand (TF); this is understandable since the latter ligand maintains large electrostatic stabilization with the di-positive TMC−FeO^{2+} moiety. However, in solution the bond energy decreases since the solvent screens the electrostatic interactions in the complex and further stabilizes the dissociated TMC^{2+} (and TF^{1-}) ion(s). ZPE correction reduces the D_{Fe-Lax} values. Entropy may contribute to further lowering of these values, but since the entropic effects due to enhanced solvation are not properly accounted for by the solvation calculations, we do not report these quantities. Nevertheless, it is apparent that the TMC(AN)FeO^{2+} complex should undergo facile ligand exchange as is indeed found experimentally.[18a] Furthermore, since the D_{Fe-AN} value is small, one may consider that ligand exchange is initiated by loss of the CH_3CN ligand.

3.2. C−H Hydroxylation Mechanisms by $^{2S+1}\mathbf{K}_L$ Species. In view of the multiple spin-state crossings in the previous study of $\mathbf{K_{N4Py}}$with cyclohexane,[28] we followed the energy profiles for all three of the spin states. The energy profile for the reaction of $^{2S+1}\mathbf{K_{N4Py}}$with cyclohexane is displayed in Figure 2 as a reference for the other processes discussed below.

Generally, in all the mechanisms the reactants form a reactant cluster ($^{2S+1}\mathbf{RC}$) followed by a transition state for H-abstraction ($^{2S+1}\mathbf{TS_H}$) that leads subsequently to an intermediate ($^{2S+1}\mathbf{I}$).

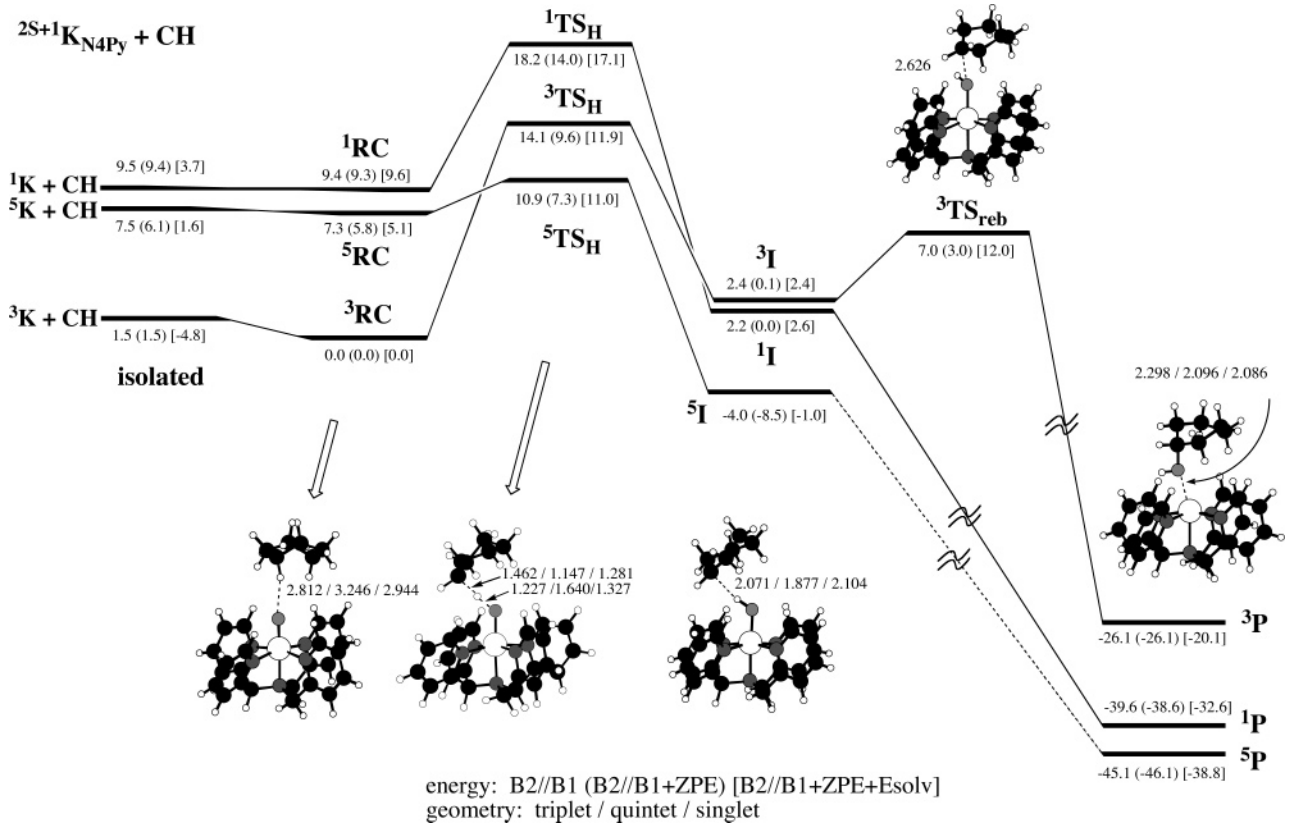

Figure 2. Energy profile for the reaction of $^{2S+1}\mathbf{K}_{\mathbf{N4Py}}$ ($S = 0, 1, 2$) with cyclohexane (**CH**). Relative energies are indicated in the order: B2//B1 (B2//B1 + ZPE) [B2//B1 + ZPE + E_{solv}]. Key bond lengths (in Å) are noted for the spin-state species, in the order: triplet/quintet/singlet.

Table 4. Barriers ($\Delta E^{\ddagger}_{H}$) and Reaction Energies ($\Delta E_{R\rightarrow I}$) for the H-Abstraction Step $^{3,5}\mathbf{K}_{\mathbf{L}}$ + RH → ^{3,5}I[a]

$\Delta E^{\ddagger}_{H}$	K_{N4Py} + CH	$K_{TMC(AN)}$ + CH	$K_{TMC(TF)}$ + CH	$K_{Bn-TPEN}$ + CH	K_{N4Py} + TE	K_{N4Py} + AN
B1: T/Q	13.1/15.8	19.3/12.0	26.9/17.7	12.1/11.2	12.8/14.5	28.5/30.9
B1+ZPE: T/Q	8.6/12.1	15.3/6.1	22.5/11.5	7.8/6.2	9.1/11.8	24.4/25.8
B2: T/Q	14.1/10.9	21.0/10.1	27.3/14.9	13.2/6.3	11.3/9.8	28.1/27.8
B2+ZPE: T/Q	9.6/7.3	17.0/4.3	22.8/8.6	8.9/1.4	7.6/7.1	24.0/22.6
B2+ZPE+solv T/Q	16.7/15.8	24.8/13.9	25.8/13.1	17.8/12.8	16.2/15.9	21.7/24.1
$\Delta E_{R\rightarrow I}$	K_{N4Py} + CH	$K_{TMC(AN)}$ + CH	$K_{TMC(TF)}$ + CH	$K_{Bn-TPEN}$ + CH	K_{N4Py} + TE	K_{N4Py} + AN
B1: T/Q	5.3/5.2	11.2/4.8	15.6/11.0	4.0/2.6	1.1/2.6	1.3/2.1
B1+ZPE: T/Q	3.0/0.8	9.1/−0.4	13.5/5.4	1.6/−2.1	−0.4/−1.1	−0.6/−1.6
B2: T/Q	2.4/−4.0	7.6/−2.0	10.7/3.2	0.9/−7.2	−5.7/−7.5	−0.5/−6.6
B2+ZPE: T/Q	0.1/−8.5	5.5/−7.3	8.6/−2.3	−1.5/−11.9	−7.2/−11.2	−2.4/−10.4
B2+ZPE+solv T/Q	7.1/3.8	11.0/2.7	12.1/2.6	6.2/0.1	0.0/0.4	5.3/2.4

[a] In kcal/mol. The gas-phase energies are relative to ^{3}**RC**. Barriers in solution are relative to $^{3,5}\mathbf{K}_{\mathbf{L}}$ + RH.

The intermediate undergoes rebound[2,28] sometimes, but not always, via a rebound TS ($^{2S+1}\mathbf{TS}_{\mathbf{reb}}$), and forms the C−O bond of the alcohol complex ($^{2S+1}$**P**). The entire data set can be found in the SI document (Tables S6, S7), while the B1/B1 and B2//B1 barrier data are collected in Tables 4 and 5. Below we describe the energy profiles, using only the corresponding B2//B1 data. Note that the reference state for gauging the gas-phase barriers is ^{3}**RC**, whereas for the barrier in solution, we use the energy of the solvated separate reactants as reference (note: the ^{3}**RC** minimum lies above the separate reactants, $^{2S+1}$**K** + RH, in a solvent).

Energy Profiles for the Reaction between $^{2S+1}\mathbf{K}_{\mathbf{N4Py}}$ and Toluene (TE). Figure 3 summarizes the relative energies and key structures along the hydroxylation reaction of $\mathbf{K}_{\mathbf{N4Py}}$ with toluene (**TE**).

Much as is found in Figure 2 above,[28] here too the reaction starts on the triplet ground state. Subsequently, the quintet $^{5}\mathbf{TS}_{\mathbf{H}}$ attains the lowest energy. We can exclude a reaction via the $^{1}\mathbf{TS}_{\mathbf{H}}$ species, which is highest in energy and does not cross the triplet surface. Focusing on the triplet surfaces in Figures 2 and 3, we can see that the gas-phase barriers (B2+ZPE relative to ^{3}**RC**) for the $\mathbf{K}_{\mathbf{N4Py}}$ with toluene vs cyclohexane are 7.6 vs 9.6 kcal/mol, respectively, while with solvation energy correction, these barriers (now relative to $^{3}\mathbf{K}_{\mathbf{L}}$ + RH) become 16.2 vs 16.7 kcal/mol. The experimental data[16] reveal a free energy barrier difference of 1.5 kcal/mol, favoring the reaction with toluene with the weaker C−H bond. As such, the triplet-state data that prefer the reaction with toluene are in accord with experiment.

Following H-abstraction, the intermediates $^{2S+1}$**I** (Figure 3) undergo rebound to form the alcohol complexes. Much as in Figure 2,[28] the C−O bond-forming process has a rebound barrier only on the triplet surface. Due to the collinear Fe···O···H···C arrangement in the quintet intermediate, a forward scan, using

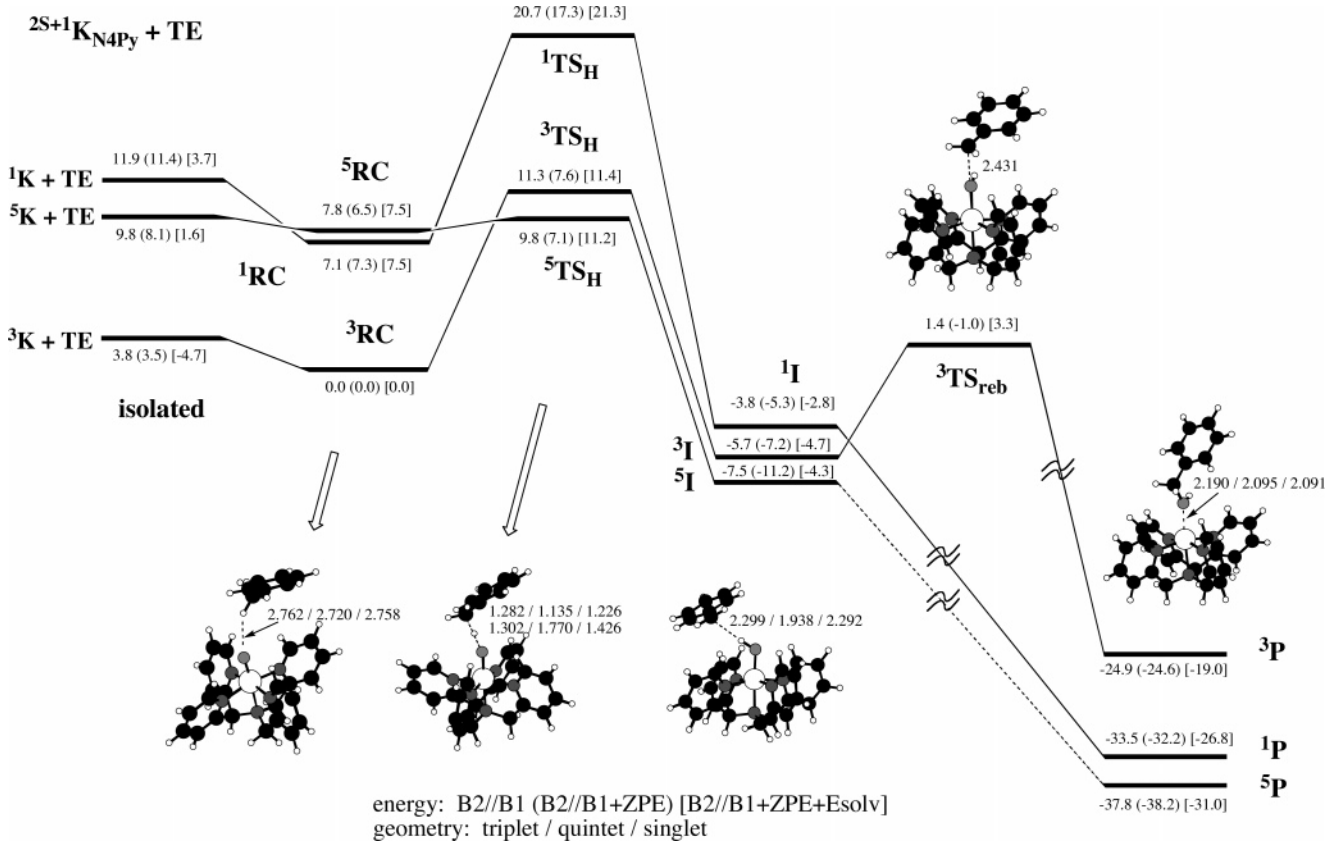

Figure 3. Energy profile for the reaction of $^{2S+1}\mathbf{K_{N4Py}}$ ($S = 0, 1, 2$) with toluene (**TE**). Relative energies are indicated in the order: B2//B1 (B2//B1 + ZPE) [B2//B1 + ZPE + E_{solv}]. Key bond lengths (in Å) are noted for the spin-state species, in the order: triplet/quintet/singlet.

Table 5. Barriers ($\Delta E^{\ddagger}_{reb}$) and Reaction Energies ($\Delta E_{I \rightarrow P}$) for the Rebound Step ^{3,5}I → ^{3,5}P (in kcal/mol)

$\Delta E^{\ddagger}_{reb}$	$\mathbf{K_{N4Py}}$ + CH	$\mathbf{K_{TMC(AN)}}$ + CH	$\mathbf{K_{TMC(TF)}}$ + CH	$\mathbf{K_{Bn-TPEN}}$ + CH	$\mathbf{K_{N4Py}}$ + TE	$\mathbf{K_{N4Py}}$ + AN
B1: T/Q	7.9/−	none	10.5/−	4.6/−	7.4/−	26.3/22.9
B1+ZPE: T/Q	6.2/−		8.9/−	3.5/−	6.6/−	26.2/22.8
B2: T/Q	4.6/−	none	11.6/−	1.9/−	7.1/−	26.4/22.8
B2+ZPE: T/Q	2.9/−		10.0/−	0.8/−	6.3/−	26.4/22.7
B2+ZPE+solv T/Q	9.7/−		9.2/−	4.2/−	8.1/−	15.3/10.5
$\Delta E_{I \rightarrow P}$	$\mathbf{K_{N4Py}}$ + CH	$\mathbf{K_{TMC(AN)}}$ + CH	$\mathbf{K_{TMC(TF)}}$ + CH	$\mathbf{K_{Bn-TPEN}}$ + CH	$\mathbf{K_{N4Py}}$ + TE	$\mathbf{K_{N4Py}}$ + AN
B1: T/Q	−25.3/−42.4	−47.1/−48.7	−36.1/−46.5	−34.8/−47.6	−20.1/−31.9	0.0/−11.3
B1+ZPE: T/Q	−23.0/−39.0	−45.9/−46.2	−35.1/−43.8	−32.7/−43.8	−18.3/−28.5	2.0/−8.1
B2: T/Q	−28.5/−41.0	−49.2/−50.8	−38.3/−49.7	−37.0/−45.5	−19.2/−30.4	−3.7/−10.1
B2+ZPE: T/Q	−26.2/−37.6	−48.0/−48.3	−37.2/−47.0	−34.9/−41.8	−17.4/−26.9	−1.7/−6.9
B2+ZPE+solv T/Q	−22.4/−37.8	−42.4/−46.9	−39.5/−48.3	−30.2/−40.6	−14.2/−26.7	−10.5/−20.7

the C−O distance as a reaction coordinate, produces an unnatural energy spike. To avoid this technical problem, we performed a backward scan starting from the product complex ^{5}**P** (Figure S6). These scans led to intermediate species with a bent Fe−O−H angle, almost identical energies to those of ^{5}**I** (except the case for $^{5}\mathbf{K_{TMC(TF)}}$; see below), and the electronic states typical to ^{5}**P**. Therefore, we used a dotted line to connect ^{5}**I** and ^{5}**P** in Figure 3. Interestingly, the rebound barrier on the triplet state is smaller than that calculated above for cyclohexane (Figure 2),[28] in accord with a recent theoretical model for the rebound process.[43] In addition, here $^{3}\mathbf{TS_{reb}}$ is significantly lower than $^{3}\mathbf{TS_{H}}$, whereas the opposite was true for the reaction of $^{5}\mathbf{K_{N4Py}}$ with cyclohexane.[28] Thus, with two "rate-determining states", the latter reaction will be further slowed by a factor of 2.

Energy Profiles for the Reaction between $^{2S+1}\mathbf{K_{N4Py}}$ and Acetonitrile. The UB3LYP/B1 calculated bond energies gave D_{C-H} (CH_3CN) = 99.6 kcal/mol and D_{C-H} (C_6H_{12}) = 101.7 kcal/mol. Why then do the iron−oxo reagents actually survive in acetonitrile? The energy profile for the reaction between $^{2S+1}\mathbf{K_{N4Py}}$ and acetonitrile is displayed in Figure 4. Similar to a recent study of the reactivity of an Fe(V)O reagent toward CH_3CN,[44] here too, the barriers for the triplet as well as quintet states are significantly higher than those in the reactions of the same reagent with cyclohexane and with toluene (Figures 2 and 3). Thus, the UB3LYP calculations reproduce the experimental finding that acetonitrile will be oxidized very sluggishly by these iron−oxo reagents.[14−18] An unusual feature in Figure 4 compared with, for example, Figure 2, is the presence of large rebound barriers for all spin states.

Energy Profiles for the Reaction between $^{2S+1}\mathbf{K_{Bn-TPEN}}$ and Cyclohexane (CH). Experimentally, $\mathbf{K_{Bn-TPEN}}$ is more reactive than $\mathbf{K_{N4Py}}$ (by a factor of 10) toward all organic

(43) Shaik, S.; Cohen, S.; de Visser, S. P.; Sharma, P. K.; Kumar, D.; Kozuch, S.; Ogliaro, F.; Danovich, D. *Eur. J. Inorg. Chem.* **2004**, *35*, 207−226.

(44) Bassan, A.; Blomberg, M. R. A.; Siegbahn, P. E. M.; Que, L., Jr. *Chem. Eur. J.* **2005**, *11*, 692−705.

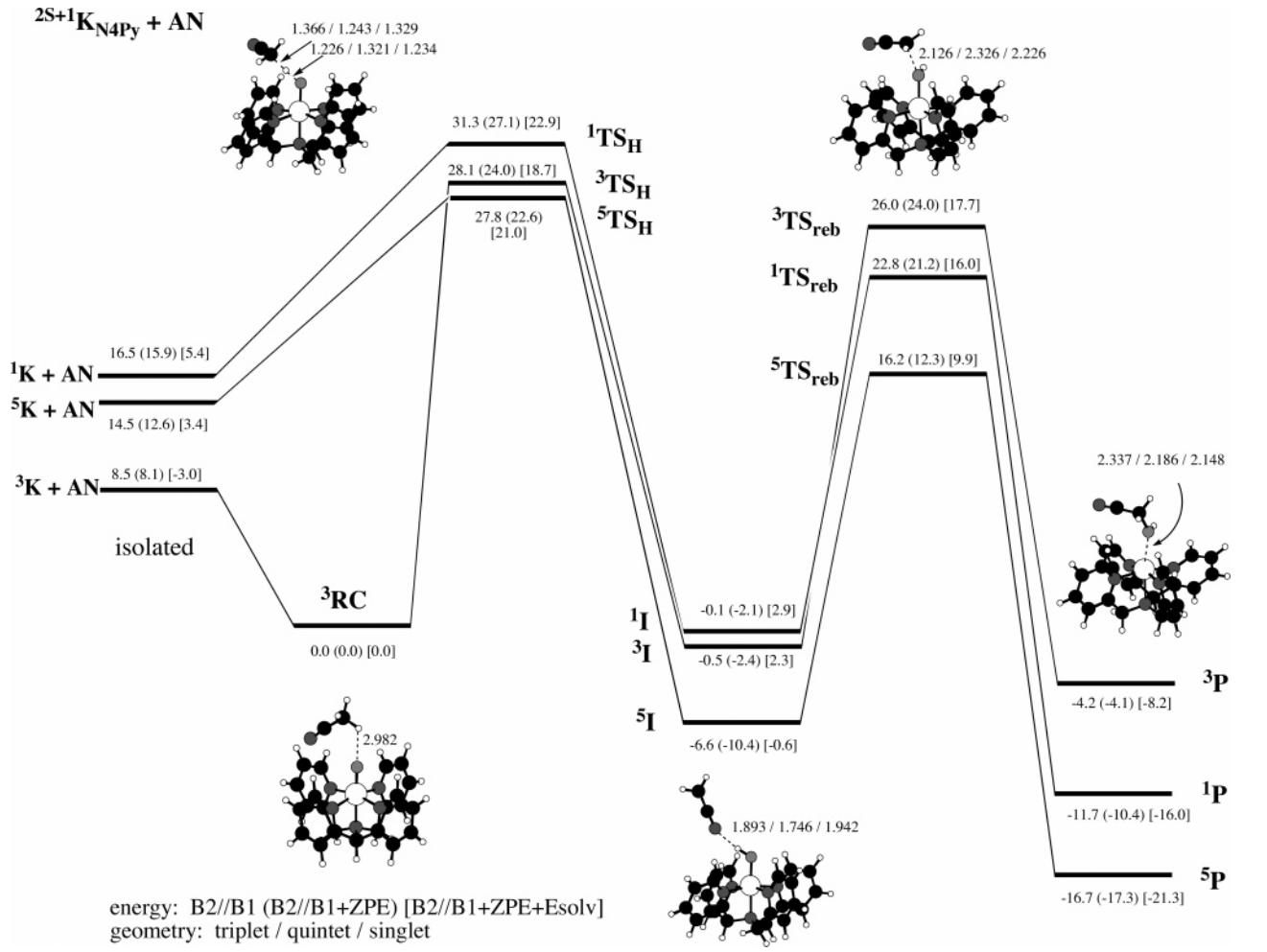

Figure 4. Energy profiles for the reaction of $^{2S+1}\mathbf{K}_{\mathbf{N4Py}}$ ($S = 0, 1, 2$) with acetonitrile (**AN**). Relative energies are indicated in the order: B2//B1 (B2//B1 + ZPE) [B2//B1 + ZPE + E_{solv}]. Key bond lengths (in Å) are noted for the spin-state species, in the order: triplet/quintet/singlet.

molecules tried by Kaizer et al.[16] To test the ability of theory to predict this trend, we studied in Figure 5 the reaction of $^{2S+1}\mathbf{K}_{\mathbf{Bn-TPEN}}$ with cyclohexane. It is seen that the general features of the energy profile are all similar to the corresponding profile with $^{2S+1}\mathbf{K}_{\mathbf{N4Py}}$ (Figure 2), with some obvious quantitative differences.[28] On the gas-phase triplet surface (B2 + ZPE, and relative to ^{3}**RC**) the barriers are lower for $\mathbf{K}_{\mathbf{Bn-TPEN}}$, while with solvent correction, the barrier order was inverted in favor of $\mathbf{K}_{\mathbf{N4Py}}$. Using a less polar solvent ($\epsilon = 5.7$ and $r = 2.72$ Å), we still found the same trend, 16.2 vs 15.3 kcal/mol, namely: $\Delta E^{\ddagger}(^3\mathbf{K}_{\mathbf{Bn-TPEN}}) > \Delta E^{\ddagger}(^3\mathbf{K}_{\mathbf{N4Py}})$. The experimental data show that the free-energy barrier for $\mathbf{K}_{\mathbf{Bn-TPEN}}$ with cyclohexane is ~1 kcal/mol lower than the corresponding one with $\mathbf{K}_{\mathbf{N4Py}}$.[16] Thus, the relative reactivity of the two oxo−iron reagents on the triplet surface is opposite to that from experimental observation. This might reflect the missing entropic factors in the calculations (e.g., solvation entropy) or simply computational inaccuracy. However, this mismatch might reflect that the actual reaction occurs by spin-state crossing to the quintet-state surface where the barriers are significantly lower for $\mathbf{K}_{\mathbf{Bn-TPEN}}$. Note also that $\mathbf{K}_{\mathbf{Bn-TPEN}}$ has a smaller rebound barrier compared with that of $\mathbf{K}_{\mathbf{N4Py}}$ (Figure 2).

Energy Profiles for the Reaction between $^{2S+1}\mathbf{K}_{\mathbf{TMC(AN)}}$ and Cyclohexane (CH). We recall that $\mathbf{K}_{\mathbf{TMC(AN)}}$ exhibits a sluggish H-abstraction reactivity.[14,18] Figure 6 displays the corresponding reaction profile of $\mathbf{K}_{\mathbf{TMC(AN)}}$ with **CH**. Comparison of the barriers for H-abstraction, with the corresponding ones in Figures 2 and 5, shows that, on the triplet surface, the reagent $\mathbf{K}_{\mathbf{TMC(AN)}}$ has by far the highest barriers among the three $\mathbf{K}_{\mathbf{L}}$ reagents. By contrast, the quintet-state surface for $^5\mathbf{K}_{\mathbf{TMC(AN)}}$ has a small barrier compared with that of $^5\mathbf{K}_{\mathbf{N4Py}}$ reagent (13.8 vs 15.8 kcal/mol with solvation energy correction). Obviously, since the $\mathbf{K}_{\mathbf{TMC(AN)}}$ reagent is a sluggish oxidant under experimental conditions, this suggests the hypothesis that a spin flip from triplet to quintet does not take place for $\mathbf{K}_{\mathbf{TMC(AN)}}$ and that the relative reactivities of $\mathbf{K}_{\mathbf{TMC(AN)}}$ and $\mathbf{K}_{\mathbf{N4Py}}$ toward cyclohexane reflect their reactivities on the triplet surfaces. A puzzling feature in Figure 6 is the lack of barriers for the rebound processes compared with Figures 2 and 5.

Energy Profiles for the Reaction between $^{2S+1}\mathbf{K}_{\mathbf{TMC(TF)}}$ and Cyclohexane (CH). Experimentally, $\mathbf{K}_{\mathbf{TMC(TF)}}$ was found to be more reactive than $\mathbf{K}_{\mathbf{TMC(AN)}}$ toward 9,10-dihydroanthracene.[18a] Since we already ruled out an electron-transfer mechanism, we tested the relative reactivity in H-abstraction toward cyclohexane. The corresponding profile for $^{2S+1}\mathbf{K}_{\mathbf{TMC(TF)}}$ is shown in Figure 7. Clearly, on the triplet surface the barrier for H-abstraction is larger than that for $^3\mathbf{K}_{\mathbf{TMC(AN)}}$ in Figure 6 above. As such, $^3\mathbf{K}_{\mathbf{TMC(TF)}}$ is expected to be a sluggish reagent, unless the spin flip to the quintet surface is enabled for this reagent, but less so for $^3\mathbf{K}_{\mathbf{TMC(AN)}}$. A similar hypothesis was made by one of us (L.Q.).[18a]

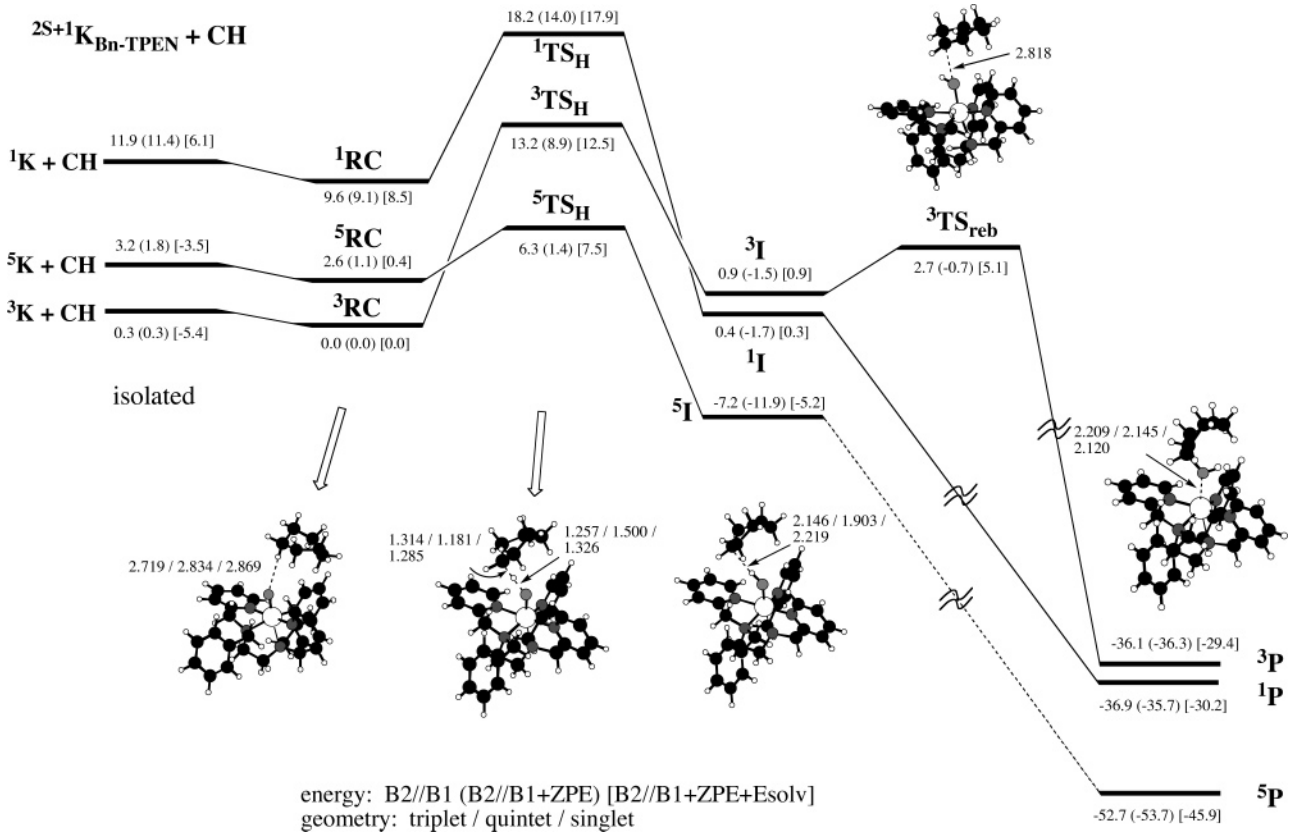

Figure 5. Energy profile along the reaction between $^{2S+1}K_{Bn-TPEN}$ ($S = 0, 1, 2$) and cyclohexane (**CH**). Relative energies are indicated in the order: B2//B1 (B2//B1 + ZPE) [B2//B1 + ZPE + E_{solv}]. Key bond lengths (in Å) are noted for the spin-state species, in the order: triplet/quintet/singlet.

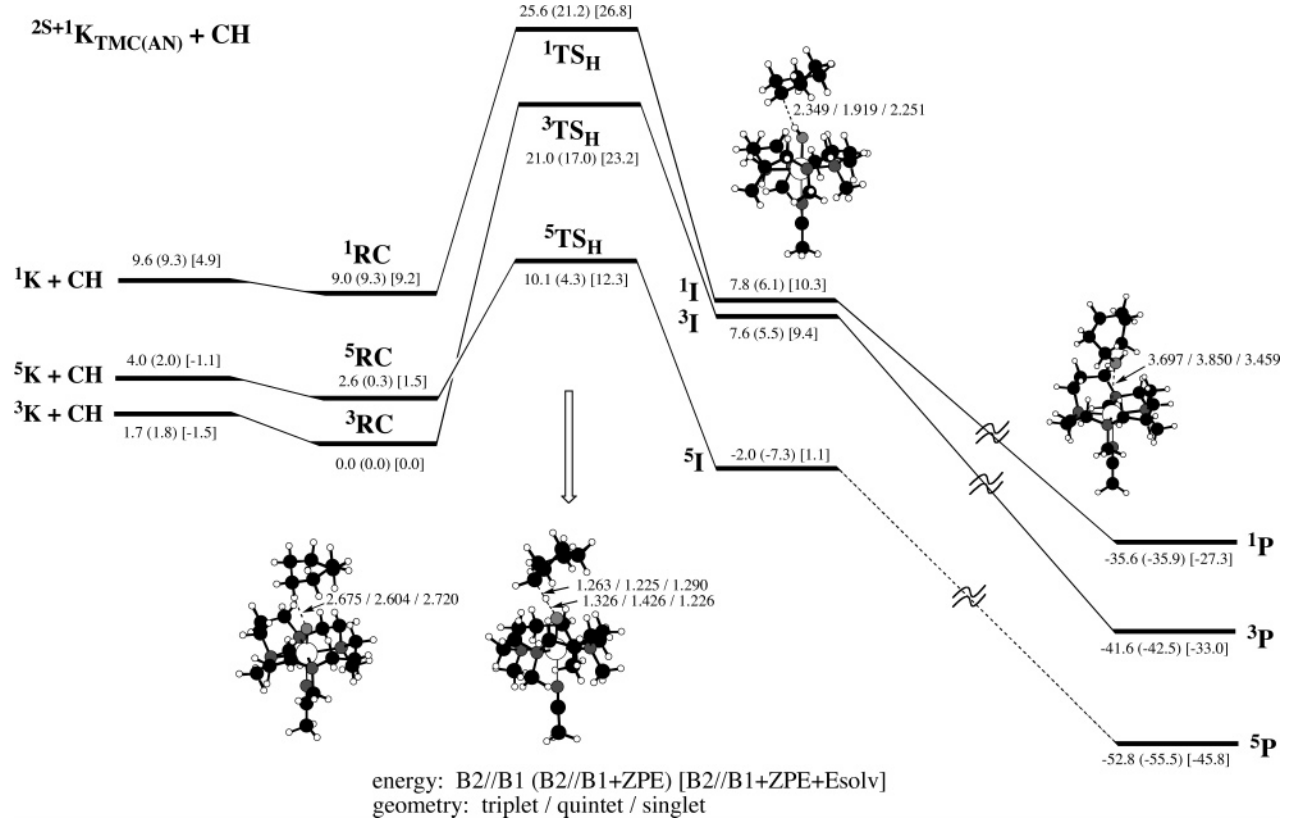

Figure 6. Energy profile along the reaction between $^{2S+1}K_{TMC(AN)}$ ($S = 0, 1, 2$) and cyclohexane (**CH**). Relative energies are indicated in the order: B2//B1 (B2//B1 + ZPE) [B2//B1 + ZPE + E_{solv}]. Key bond lengths (in Å) are noted for the spin-state species, in the order: triplet/quintet/singlet.

Studies of the Lowest-Energy Spin-State Crossing Paths. We probed the spin-state crossing starting from the ^3TS_H and ^5TS_H structures in the reactions of $^{2S+1}K_{TMC(Lax)}$ with **CH**, where crossing occurs at the UB3LYP/B1 level. With either

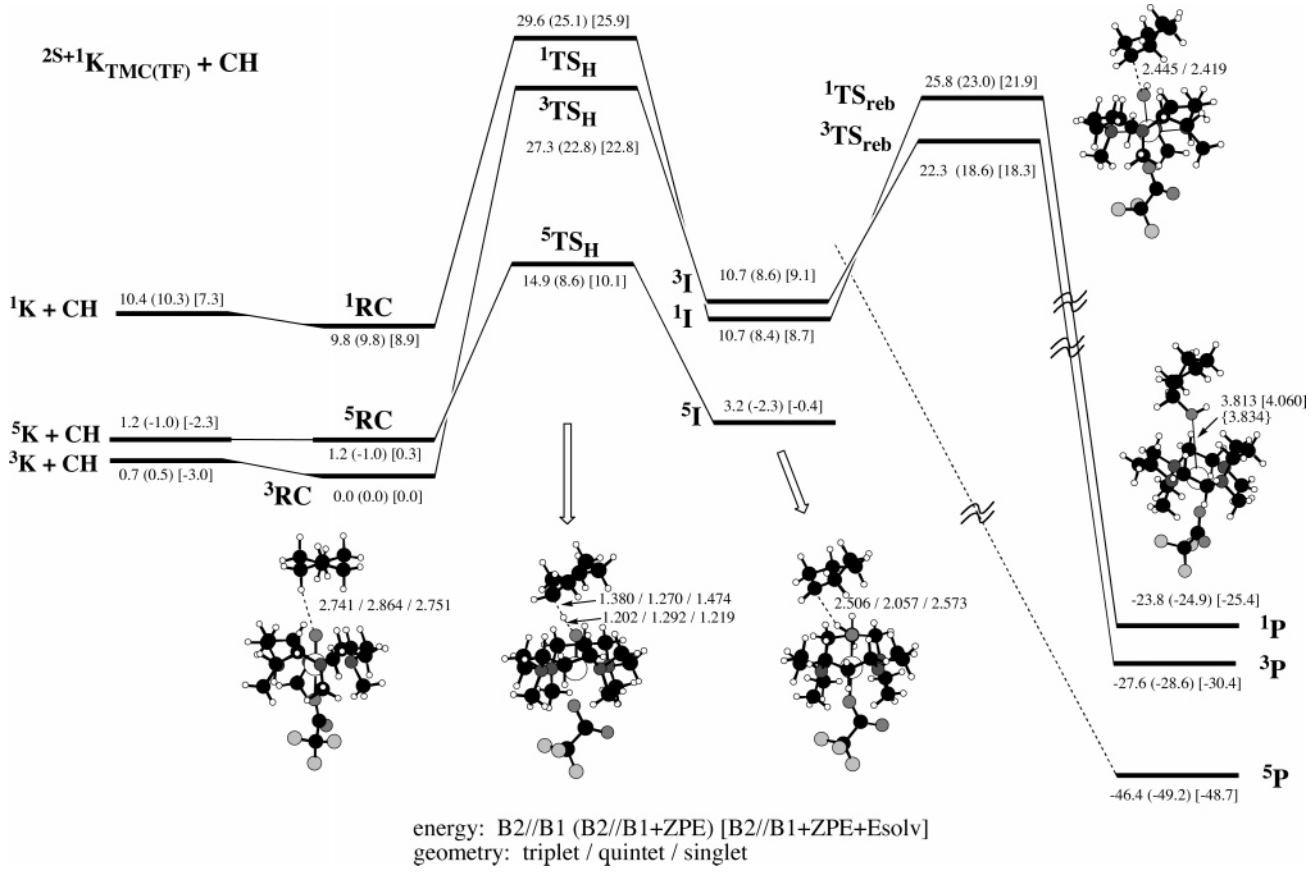

Figure 7. Energy profile along the reaction between $^{2S+1}\mathbf{K}_{\mathbf{TMC(TF)}}$ ($S = 0, 1, 2$) and cyclohexane (**CH**). Relative energies are indicated in the order: B2//B1 (B2//B1 + ZPE) [B2//B1 + ZPE + E_{solv}]. Key bond lengths (in Å) are indicated for the spin-state species, in the order: triplet/quintet/singlet.

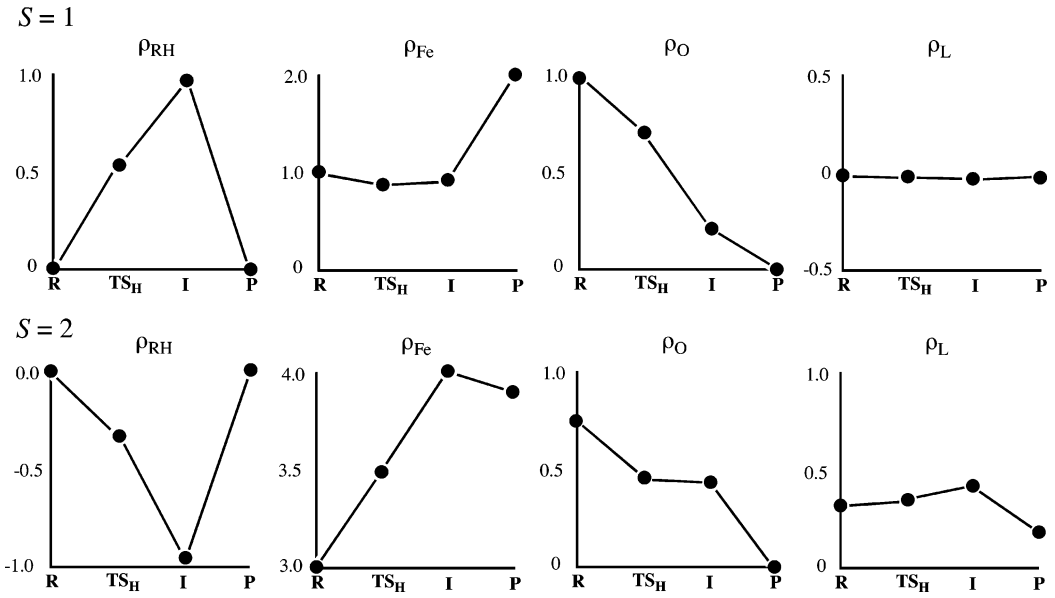

Figure 8. Spin density (ρ) development during the oxidation of RH by $^{3,5}\mathbf{K}_{\mathbf{L}}$.

starting point, the minimum-energy crossing point was near the geometry of the free reagent, and the seams of crossing ranged over the entire H-abstraction profile (Figure S3 in the SI). Thus, spin-state crossover may occur either at the geometry of the starting reagent or en route to $^5\mathbf{TS_H}$. This will depend on the probabilities of crossover as will be discussed later.

4. General Reactivity Patterns in the Data Set

Although the singlet state approaches the other two spin-state surfaces at the intermediate stage ($^{2S+1}\mathbf{I}$), until that point the singlet lies well above the other two states; hence, our foregoing discussion will focus on the triplet and quintet states. To render this discussion manageable, we collected the data in a few figures and tables, as follows: Figure 8 shows the spin density

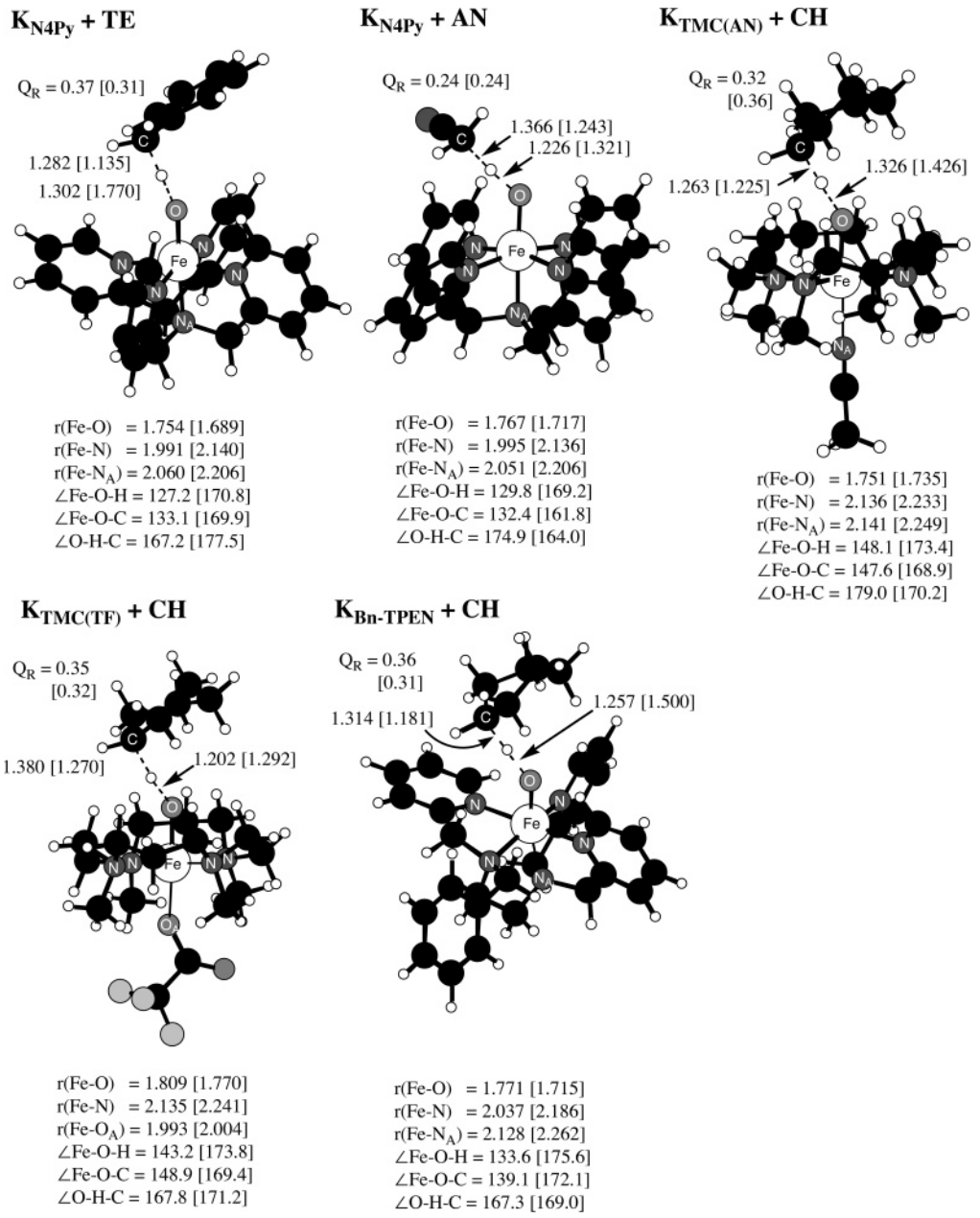

Figure 9. Geometric details and charges developed on the organic molecule (Q_R) in the H-abstraction transition states. Each datum is given two numbers corresponding to triplet [quintet], respectively.

variation along the reaction pathway for the two spin states. Detailed geometric features of the transition states for C−H cleavage and charge development on the organic molecules in these $\mathbf{TS_H}$ species are collected in Figure 9. Figure 10 shows the corresponding rebound $\mathbf{TS_{reb}}$ structures. Table 4 assembles all the data for the barriers for H-abstraction on the two spin-state surfaces, while Table 5 shows the corresponding rebound barriers.

4.1. The Mechanism of Activation in the Reactions of $^{3,5}\mathbf{K_L}$ with RH. The mechanism of activation in Figures 2−7 is uniform (other triplet and quintet species were tried and found to be higher in energy than the ones in Figures 2−7; see Table S6(f)), and the key features can be understood by inspecting the spin density development along the reaction paths, as depicted in Figure 8. The triplet state reveals that the organic molecule (RH) develops a radical character that peaks at the intermediate stage and then vanishes as the R−OH bond is made. At the same time the spin on the iron ion climbs from 1 to 2, while the spin on the oxo atom diminishes from 1 to 0. On the quintet surface, there are similarities and differences with the triplet surface. The first difference is the negative spin density that develops on the organic molecule, reaching −1 at the intermediate stage; the second difference is the jump in the iron spin density from 3 to 4, and the third, the spin density on the multidentate ligands is now more pronounced compared with that in the triplet process.

These changes can be represented by a corresponding orbital occupancy evolution in Scheme 3 using the oxidation state formalism.[45] Thus, initially on the triplet surface, the occupancy of $^3\mathbf{K_L}$ involves two electrons in π^* orbitals that are both antibonding FeO orbitals and hence distribute the two spins

(45) Shaik, S.; de Visser, S. P. In *Cytochrome P450: Structure, Mechanism, and Biochemistry*, 3rd ed.; Ortiz de Montellano, P. R., Ed.; Plenum Publishing: New York, 2004; pp 45−85.

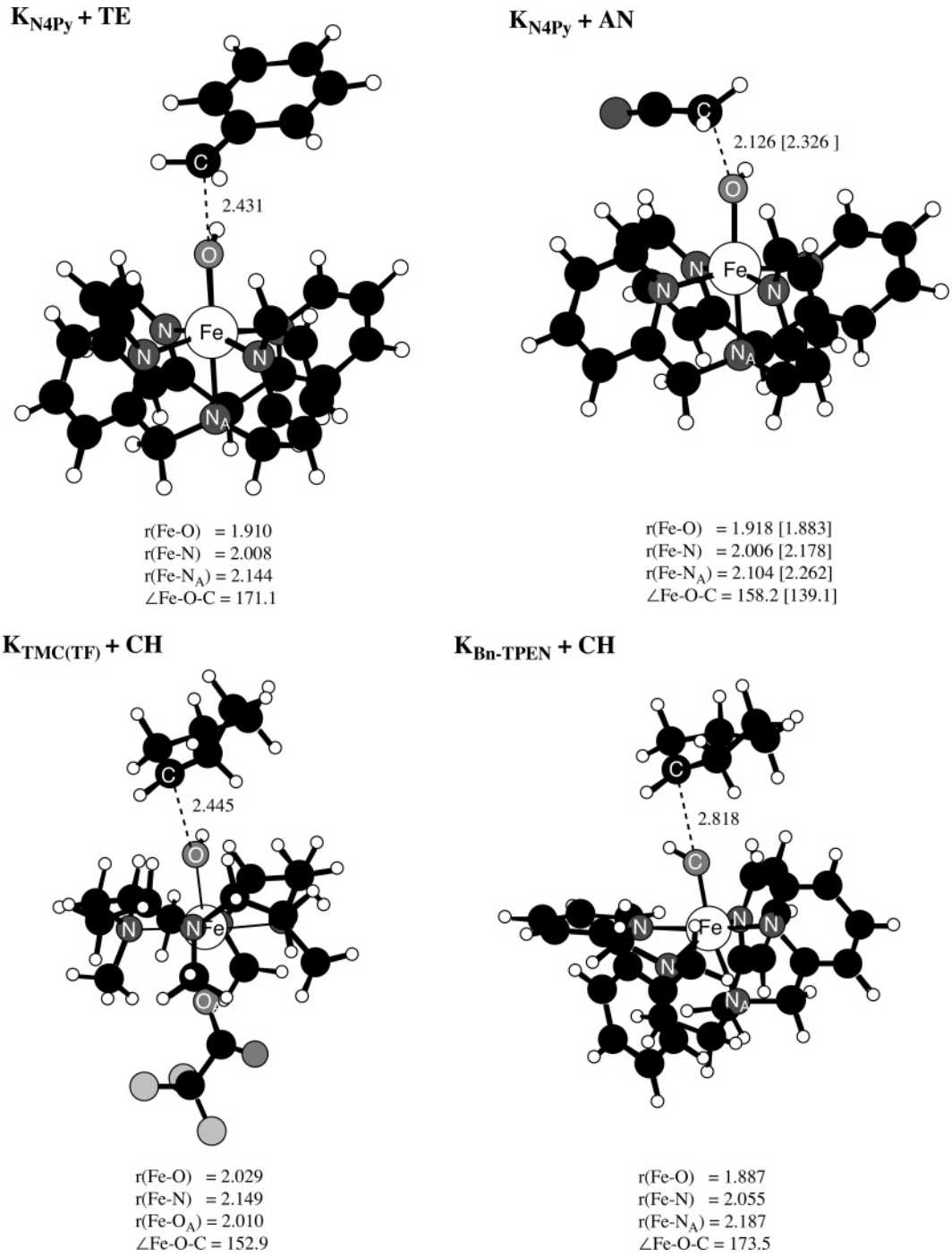

Figure 10. Geometric details of the rebound transition states in this study. Wherever available, each datum is given two numbers corresponding to triplet/[quintet], respectively.

equally: one on Fe and the other on O. As H-abstraction occurs, one electron (with spin-down) shifts from the σ_{CH} orbital of the substrate to a π^* orbital of the iron−oxo reagent; as a result, the spin on the oxo is depleted due to the O−H bond formation (and appearance of σ_{OH} and σ^*_{OH} orbitals) while spin develops on the organic molecule that now possesses a singly occupied orbital (ϕ_C). At the same time, the spin density on iron remains almost constant since the singly occupied π^* orbital acquires a dominant iron d-character. In the end, the orbital of the organic moiety (ϕ_C) combines with the oxygen orbital of the remaining π_{FeO}, and they evolve together to become the σ_{CO} and σ^*_{CO} orbitals of the alcohol.

On the quintet surface, the electron that shifts initially from σ_{CH} is a spin-up electron, and hence the spin density that develops on the organic molecule is negative, reaching −1 at the intermediate stage. The electron shifts into the $\sigma^*_{z^2}$ orbital of iron−oxo, and hence the spin density on Fe jumps from 3 to 4 at the intermediate stage. In fact, there are now five unpaired electrons in ^{5}**I**; however, since the corresponding d orbitals are delocalized (see e.g., Scheme 2), the total spin is only 4. Since all the d orbitals are occupied and since both σ^*_{xy} and $\sigma^*_{z^2}$ orbitals involve ligand contribution, the spin density on the multidentate ligand increases and then drops at the product stage when the δ orbital gets filled.

Scheme 3. Orbital Diagrams Showing the Evolution in d-Orbital Occupancy along the Oxidation Pathway; Both π and π^* Orbitals Involve Initially the Fe=O Moiety[46]

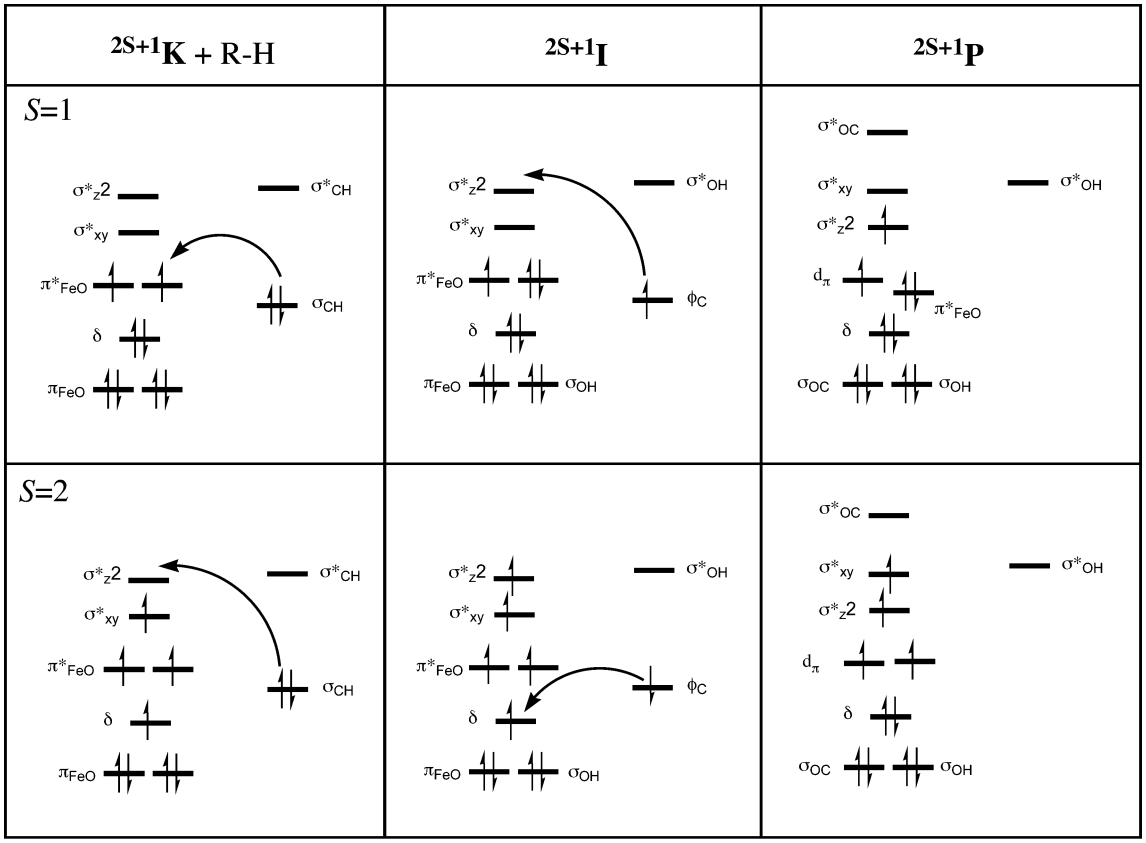

This orbital picture accounts also for special structural characteristics of the ^{3,5}**TS$_H$** species in Figure 9. Thus, when an electron shifts from the σ_{CH} orbital of the organic molecule to some orbital of the iron−oxo reagent, *the two reactants will assume a transition structure that optimizes the interaction between the two orbitals, as much as possible*.[47,48] Accordingly the FeOH (FeOC) angles are ∼120° for the triplet transition state, since on the triplet surface the electron shift is to the π^* orbital (the deviation from 90° reflects the optimization of the overlap by avoiding the node in the π^*_{FeO} orbital). By contrast, these angles for the quintet species are ∼170°, since on this surface the shift occurs to the $\sigma^*_{z^2}$ orbital that lies on the Fe−O axis, thus requiring the H-abstraction to occur along the FeO bond axis. Further support for the simple orbital picture comes from the rebound transition states in Figure 10. It is seen that the trends in the FeOC angles in ^{3,5}**TS$_{reb}$** are opposite to those discussed for ^{3,5}**TS$_H$**. Thus, in the triplet ^{3}**TS$_{reb}$** the angle is 153−174°, reflecting that the second electron shift (Scheme 3) occurs from the orbital of the organic radical to the $\sigma^*_{z^2}$ orbital and is dictated by maximum overlap requirement between the ϕ_C and $\sigma^*_{z^2}$ orbitals. By contrast, in the ^{5}**TS$_{reb}$** the electron shift is to the δ orbital, and the FeOC angle is accordingly smaller.

4.2. Trends in the Activation Barriers. Table 4 shows the corresponding data for the H-abstraction step, while Table 5 collects the data for the rebound step.

Trends in the H-Abstraction Barriers. The barriers in Table 4 exhibit a few trends. First, in most reactions, solvation raises the barriers relative to the gas-phase values. The solvent effect arises due to the stronger solvation of the doubly positive ^{3}**K$_L$**$^{2+}$ reagent compared with the corresponding ^{3,5}**TS$_H$** species where the charge is diffused over the reagent and the organic molecule. Second, considering that the barrier for the quintet-state reaction is gauged from the lowest point on the triplet ground-state surface (^{3}**RC** in the gas phase, ^{3}**K$_L$** + RH in solution phase), the net barrier on the quintet surface is extremely small (consult Figures 2−7), and the corresponding ^{5}**TS$_H$** species are also very early (inspect the r_{OH} and r_{CH} distances in Figure 9). In fact, much of the quintet barrier is due to the solvation effect. The orbital evolution diagram in Scheme 3 shows that the quintet-state barrier is due to the fact that in the ^{5}**TS$_H$** species a spin-up electron initially in the organic molecule shifts to the $\sigma^*_{z^2}$ orbital. As a result, the exchange stabilization in the d-block orbitals is enhanced by five exchange interactions, and since d−d exchange interaction for iron is significant,[25,42] the **TS$_H$** species attains low energies.

Considering the triplet surface, in the gas phase the relative reactivity of the ^{3}**K$_L$** reagents, with respect to a given organic molecule (**CH**), is the following: L = Bn-TPEN > N4Py ≫ TMC(AN) > TMC(TF), irrespective of the basis set. The solvent changes this trend to: L = N4Py > Bn-TPEN > TMC(TF) > TMC(AN). As we already noted, the solvent effect is large, and hence, the gas-phase order, Bn-TPEN > N4Py, is reversed in solution, reflecting the stronger solvation of the ^{3}**K$_{Bn-TPEN}$** reagent, in which the FeO unit is more exposed to the solvent compared with other cases. We note that the gas-phase trends are in better agreement with experimental data than the solution-phase trends. Nevertheless, both gas-phase and solution data

(46) In the case of TMC(AN) the rebound involves electron shift to π^*.
(47) Shaik, S.; Shurki, A. *Angew. Chem., Int. Ed.* **1999**, *38*, 586−625.
(48) Kumar, D.; de Visser, S. P.; Sharma, P. K.; Hirao, H.; Shaik, S. *Biochemistry* **2005**, *44*, 8148−8158.

Scheme 4. UB3LYP/B1 Computed Adiabatic and in-Situ C−H Bond Dissociation Energies (D_{R-H}'s) and Radical Ionization Potentials ($IP_{R\bullet}$, Given as Gas-Phase [Solution-Phase] Values); Data in kcal/mol; Radical Structures Were Taken from ^{3}I

	H-CH_2CN	H-C_6H_{11}	H-CH_2Ph
D_{R-H}	99.6	101.7	94.5
$D_{R-H}^{in-situ}$	112.0	109.9	107.6
$IP_{R\bullet}$	236.5 [165.9]	166.2 [107.7]	161,5 [110.2]

show that the TMC(L_{ax}) ligands are the least reactive, in accord with experiment. Inspection of the barriers vis-à-vis the H-abstraction energies ($\Delta E_{R\rightarrow I}$), shows that there is a correlation between the two quantities, as expected from the Bell−Evans−Polanyi principle.[49] Interestingly, as recently shown,[28] the H-abstraction energies do not reflect only variation in the relative strengths of the formed O−H bond for the different reagents but also the significant electrostatic interaction between the cyclohexyl radical and the positively charged reagent; some of this stabilization carries over to the ^{3}**TS$_H$** species and thereby affects the barrier. The solvent screens these interactions and stabilizes the reactant state, making all the reactions thermoneutral/endothermic, $\Delta E_{R\rightarrow I} = 0.0-12.1$ kcal/mol, and changing the stability trends and hence also the barrier trends. It is still puzzling, however, that the trends of the triplet-state solution barriers do not fully conform to experimental trends; possible causes for the deviations are addressed later.

For a given ^{3}**K$_L$** reagent (N4Py), the organic molecules exhibit the following reactivity trend: toluene(**TE**) > cyclohexane(**CH**) > acetonitrile(**AN**), in both the gas phase and solution. While this trend accords with experimental findings, still it is puzzling why should acetonitrile, which possesses a C−H bond dissociation energy even smaller than that in cyclohexane, have a much higher barrier? As we argued recently,[50] the adiabatic bond dissociation energy involves the reorganization energy of the corresponding radical,[44] and a more appropriate predictor of reactivity[47] is the "in situ" bond dissociation energy that leaves the radical in its geometry as in the molecule. In addition, as in every H-abstraction transition state, part of the stabilization of the species comes from the mixing in of the polar R^+ $^\bullet$H:O^- resonance structure.[47] This stabilization by the "polar effect" will depend critically on the ability of R• to donate an electron and, hence, on the ionization potential (IP) of the radical. Scheme 4 shows these quantities for the three substrates studied here. It is seen that, while the adiabatic C−H bond energy of acetonitrile is smaller than that of cyclohexane, the in situ value is larger. In addition, judging from the $IP_{R\bullet}$ quantities, the $NCCH_2^\bullet$ moiety will exert the smallest polar effect and smallest stabilization of the corresponding **TS$_H$**.

Turning now to the rebound barriers in Table 5, we can see a general trend, namely in most cases the quintet surface has no rebound barrier, and when the barrier is present it is smaller than the barrier on the triplet surface. It is seen that generally, the quintet-rebound process is more exothermic than the corresponding triplet process. The reasons for both features become clear from the orbital evolution diagram in Scheme 3. Thus, the quintet surface involves an electron shift from the radical orbital (ϕ_C) to the lowest orbital in the d-block, δ. By contrast, on the triplet surface, the electron is shifted to the highest-lying $\sigma^*_{z^2}$ orbital (which then relaxes at the product stage). Consequently, the triplet rebound is less exothermic and has a significant barrier, while the quintet reaction is generally *effectively concerted*.

Scheme 5. UB3LYP/B1 Computed Electron Affinities (EA_{FeOH}) of Ferric−Hydroxo Complexes; Structures Were Taken from ^{3}I

	TMC(AN)$FeOH^{2+}$	Bn-TPEN$FeOH^{2+}$	N4Py$FeOH^{2+}$	TMC(TF)$FeOH^{2+}$
EA_{FeOH}	174 (70)	161 (68)	164 (69)	99 (62)

Another trend concerns the dependence of the triplet-rebound barrier on the nature of the radical (R•). Thus, the barrier behaves in the following order: $\Delta E^{\ddagger}_{reb}$ ($PhCH_2^\bullet$) < $\Delta E^{\ddagger}_{reb}$ ($C_6H_{11}^\bullet$) < $\Delta E^{\ddagger}_{reb}$ ($NCCH_2^\bullet$). At the same time, the respective reaction becomes less exothermic as the radical varies from $PhCH_2^\bullet$ to $NCCH_2^\bullet$. Following the orbital evolution diagram (Scheme 3), it is seen that the rebound involves a shift of an electron from the radical orbital (ϕ_C) to the ferric−hydroxo complex. Therefore, it is expected that the rebound barrier will follow the ionization potential of the radical, $IP_{R\bullet}$.[43,44] The $IP_{R\bullet}$ data in Scheme 4 provides a clear explanation for the variation of the rebound barrier in these three radicals. Finally, for a given radical one can see that $\Delta E^{\ddagger}_{reb}$ (TMC(AN)) < $\Delta E^{\ddagger}_{reb}$ (Bn-TPEN) < $\Delta E^{\ddagger}_{reb}$ (N4Py) < $\Delta E^{\ddagger}_{reb}$ (TMC(TF)). The data in Scheme 5 show that, with one exception (the barriers of Bn-TPEN vs N4Py), the electron affinities of the iron−hydroxo species predict the trend: the better acceptor is the ferric hydroxo complex, the smaller is the rebound barrier.

4.3. The Question of Two-State Reactivity (TSR) in the Reactions of Non-Heme Iron(IV)−Oxo Reagents. As we already noted, some trends cannot be accounted for in terms of a reaction on the triplet-state surface. For example, the relative reactivity of ^{3}**K$_{Bn-TPEN}$** and ^{3}**K$_{N4Py}$**, which in solution is calculated to be opposite to the experimental data, and relative reactivities of ^{3}**K$_{TMC(AN)}$** and ^{3}**K$_{TMC(TF)}$**, which are also reversed compared with those from experiment. These reversals may be the results of inaccuracies in the calculations or due to unaccountable entropic effects of solvation. However, they can be understood if one invokes TSR via crossover to the quintet-state surface.[28] The likelihood of such a crossover seems significant in view of the fact that the spin-state surfaces are so close and cross throughout the H-abstraction pathway (Figure S3). As such, it is essential to consider this possibility and to make some predictions for distinguishing a single-state reactivity (SSR) on the triplet surface from cases where TSR takes place.[51] The calculations of the minimum-energy crossing point showed that the region of minimum energy is the free ^{5,3}**K$_L$** reagents, but there are low-energy crossing points also en route to ^{5}**TS$_H$**. As such, one may think about two mechanistic scenarios that are depicted in Scheme 6. In the first mechanism, in Scheme 6a, a change in the geometry of the triplet complex ^{3}**K$_L$** in the direction of the quintet-complex geometry, causes crossing between the two states. Thereafter, the reaction can proceed on the quintet surface or bifurcate again to the triplet surface as shown schematically by the arrows. Scheme 6b describes scenarios where the crossing occurs en route to ^{5}**TS$_H$**.

A situation belonging to Scheme 6a (**Case A**) will occur when the ^{3}**K$_L$** − ^{5}**K$_L$** energy gap is very small so that there is spin-

(49) Mayer, J. M. *Acc. Chem. Res.* **1998**, *31*, 441−450.
(50) de Visser, S. P.; Kumar, D.; Cohen, S.; Shacham, R.; Shaik, S. *J. Am. Chem. Soc.* **2004**, *126*, 8362−8363.
(51) (a) Shaik, S.; Danovich, D.; Fiedler, A.; Schröder, D.; Schwarz, H. *Helv. Chem. Acta* **1995**, *78*, 1393−1407. (b) Schröder, D.; Shaik, S.; Schwarz, H. *Acc. Chem. Res.* **2000**, *33*, 139−145.

Scheme 6. Mechanistic Scenarios for Spin-State Crossing: (a) A Case of Spin-State Preequilibrium (Case A); (b) Crossing in the Tunneling Region en Route to ^5TS_H (Cases B and C)

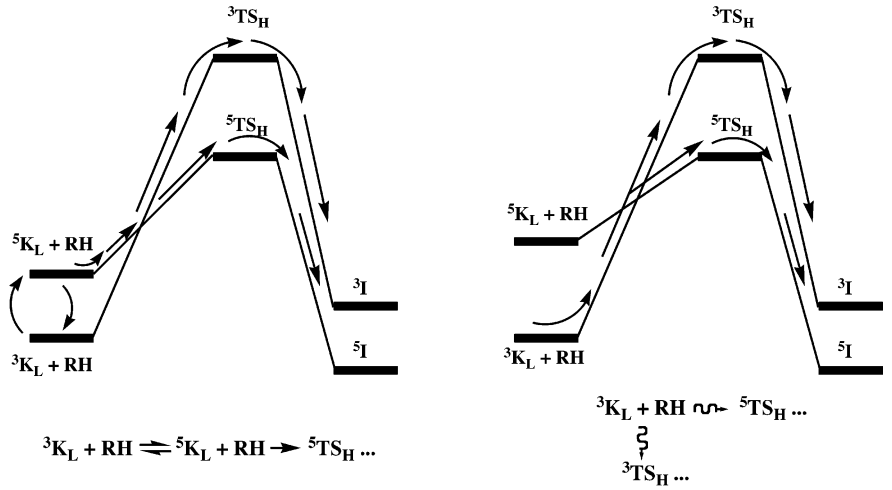

state preequilibrium followed by activation on the quintet surface. In this case, the effective barrier of the reaction will simply be given by the energy difference between the quintet transition state and the triplet ground state of the reagent, eq 1:

$$\Delta E_H^{\ddagger} = E(^5\mathbf{TS_H}) - E(^3\mathbf{K_L}+\mathrm{RH}) \qquad (1)$$

Since the spin forbiddenness affects the forward and reverse transitions of the $^3\mathbf{K_L} - {}^5\mathbf{K_L}$ preequilibrium, there will be no special effects due to spin-state transitions,[52,53] unless the probabilities of spin crossover will be so low that spin equilibrium will be established slowly. Such a crossover will lower the barrier for bond activation, and since most of the quintet-state reactions have no rebound barrier, the *spin-state will also induce an effectively concerted hydroxylation mechanism.*

In the cases described in Scheme 6b, the triplet species cross over to the quintet surface en route to $^5\mathbf{TS_H}$ in the tunneling regime.[54] Here, the crossover will be determined by the probability of transition from the triplet to the quintet.[52−56] One can then express the TSR rate constant in terms of the individual rate constants on the two surfaces multiplied by their probabilities:

$$k_r = p_{TQ}k_Q + (1 - p_{TQ})k_T \qquad (2)$$

Thus, the reaction rate constant is a sum of the rate on the quintet surface (k_Q) times the probability of triplet−quintet crossover (p_{TQ}), and the rate on the triplet surface (k_T) multiplied by its own probability ($1 - p_{TQ}$). There are two possible cases.

Case B. Whenever the quintet transition state is much lower than that of the triplet species (i.e., when $k_Q \gg k_T$) and when the probability p_{TQ} is not too small, the rate constant will be dominated by the first term, and the mechanism will occur by spin-state crossover followed by a quintet-state reaction. Since the crossover here is en route to $^5\mathbf{TS_H}$, then *the spin flip occurs in synchronicity with H-atom tunneling through the triplet barrier*. One may expect then to find a kinetic isotope effect ($KIE_{H/D}$) typical of tunneling. In addition, this scenario on the quintet surface will involve effectively concerted hydroxylation and will reveal radicals that possess ultrashort lifetimes. According to the Landau−Zener theory, spin transitions would slow as temperature increases.[52,55] As such, Case B situations may exhibit inverse *T*-dependence of rate and $KIE_{H/D}$ values; a drop of $KIE_{H/D}$ to normal values is an interesting possibility.

Case C. When the quintet transition state is close in energy to the triplet species and/or the probability p_{TQ} is very small, then spin crossover will be ineffective, and the reactivity will be dominated by the triplet surface. On the triplet surface we expect normal $KIE_{H/D}$ and stepwise mechanisms with radicals that can rearrange and lose stereochemical labels originally encoded into the RH molecule, as amply demonstrated in P450 chemistry.[1,2,43,45,57]

Intermediate Cases. Of course, some cases may involve similar contributions from the two processes in eq 2. These processes will take characteristics of the two cases.

In **Case A**, spin preequilibrium requires a small triplet−quintet energy gap at the origins. On the basis of the B2//B1 energy gaps (Figure 1) the facility of the spin equilibrium would obey the following order: $\mathbf{K_{TMC(TF)}} \approx \mathbf{K_{Bn-TPEN}} > \mathbf{K_{TMC(AN)}} > \mathbf{K_{N4Py}} > \mathbf{K_{TMC}}$; that is, it would be hardest for the complex with the TMC ligand and the vacant axial position and easiest for the TMC(TF) ligand. If the $\mathbf{K_{TMC(AN)}}$ complex can lose the AN ligand easily (Table 3), the state crossover in this complex will be the least likely. As we already noted, the recent finding (that $\mathbf{K_{TMC(TF)}}$ is more reactive than $\mathbf{K_{TMC(AN)}}$ toward H-abstraction from 9,10-dihydroanthracene[18a]) is not reproduced by the triplet-state barrier data (Table 4). If the trends of the calculations are correct, then a possible explanation for the

(52) Danovich, D.; Shaik, S. *J. Am. Chem. Soc.* **1997**, *119*, 1773−1786.
(53) For some applications and generalizations in organometallic chemistry see: (a) Harvey, J. N.; Aschi, M. *Faraday Discuss.* **2003**, *124*, 129−143. (b) Poli, R.; Harvey, J. N. *Chem. Soc. Rev.* **2003**, *32*, 1−8. (c) Harvey, J. N.; Poli, R.; Smith, K. M. *Coord. Chem. Rev.* **2003**, *238*, 347−361.
(54) Harvey, J. N.; Grimme, S.; Woeller, M.; Peyerimhoff, S. D.; Danovich, D.; Shaik, S. *Chem. Phys. Lett.* **2000**, *322*, 358−362.
(55) Schröder, D.; Schwarz, H.; Clemmer, D. E.; Chen, Y.; Armentrout, P. B.; Baranov, V.; Bohme, D. K. *Int. J. Mass. Spectrom. Ion Processes* **1997**, *161*, 175−191.
(56) For a recent comprehensive review, see: Schwarz, H. *Int. J. Mass. Spectrom.* **2004**, *237*, 15−105.
(57) Shaik, S.; Kumar, D.; de Visser, S. P.; Altun, A.; Thiel, W. *Chem. Rev.* **2005**, *105*, 2279−2328.

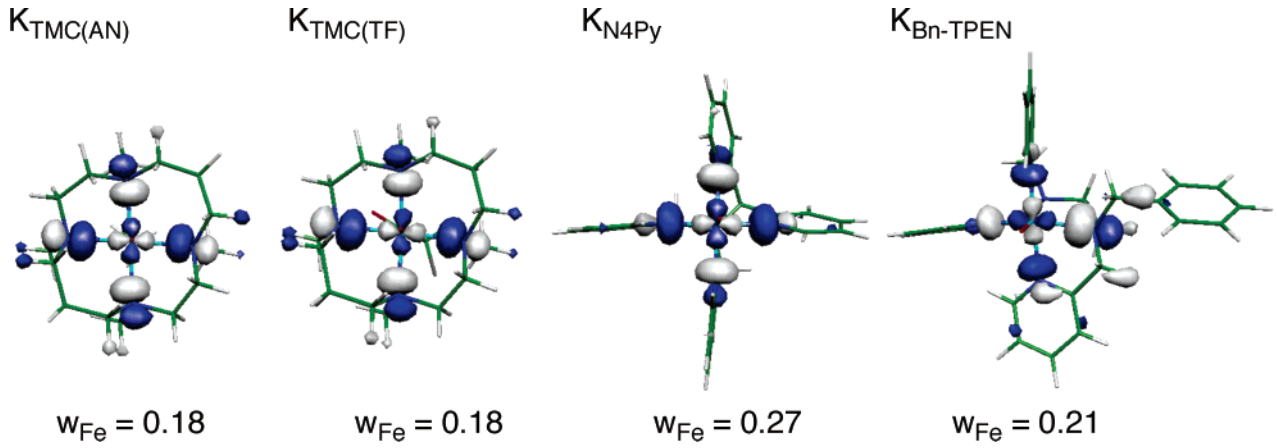

Figure 11. σ^*_{xy} orbitals and the weights of the iron d-AOs in the orbitals for $^5\mathbf{K_L}$ complexes.

experimental finding is that some of the process proceeds via the quintet surface with spin preequilibrium for the $\mathbf{K_{TMC(TF)}}$ reagent.

Cases B and **C** require consideration of the relative energy for the $^3\mathbf{TS_H}$ and $^5\mathbf{TS_H}$ species as well as the probabilities of spin crossover, p_{TQ}. It is seen (Table 4) that $\mathbf{K_{N4Py}}$ has $^3\mathbf{TS_H}$ and $^5\mathbf{TS_H}$ species of almost equal height (for the reactions with **CH**, **TE**, and **AN**), so that TSR will not greatly affect the reaction rate. As such, we may expect that the reactions of $\mathbf{K_{N4Py}}$ will proceed as in **Case C**, namely mostly on the triplet-state surface, especially if the p_{TQ} is small. On the other hand, $\mathbf{K_{Bn-TPEN}}$ has a significant $^3\mathbf{TS_H}$ and $^5\mathbf{TS_H}$ gap even with the less reactive substrate, **CH**, and is likely to have a gap similar to that for the reaction with **TE**. Therefore, $\mathbf{K_{Bn-TPEN}}$ may benefit from TSR and will belong to **Case B**, provided the crossover probability, p_{TQ}, is not extremely small. Similarly, the reactions of $\mathbf{K_{TMC(TF)}}$ and $\mathbf{K_{TMC(AN)}}$ with **CH** have significant $^3\mathbf{TS_H}$ and $^5\mathbf{TS_H}$ gaps, and may qualify for **Case B**, under the same conditions. Let us then discuss the p_{TQ} quantity.

Among the factors that affect the magnitude of p_{TQ} is the spin−orbit coupling (SOC) interaction between the states.[52,54] Thus, since during spin flip, the electron in the δ orbital in the triplet state shifts to the σ^*_{xy} orbital, the SOC between the states would be maximized when both orbitals are localized on iron.[52] While the δ orbital is fairly localized, the σ^*_{xy} orbital is delocalized toward the adjacent nitrogen atoms of the ligand (see also Table S8). As shown in Figure 11 the weight of the iron character of this orbital is rather small and is the smallest for the $\mathbf{K_{TMC(Lax)}}$ ligands and largest for $\mathbf{K_{N4Py}}$ and $\mathbf{K_{Bn-TPEN}}$. The decreased iron weight of the σ^*_{xy} orbital will decrease the initial SOC. Further decrease of SOC will occur along the reaction path. Thus, as can be seen from the orbital evolution diagram in Scheme 3, en route to the H-abstraction transition states, the RH molecule shifts an electron to the π^* orbital in the case of $^3\mathbf{TS_H}$ and to the $\sigma^*_{z^2}$ orbital in the case of $^5\mathbf{TS_H}$. Consequently, the triplet and quintet wave functions will differ now by more than a single electron occupancy, and the value of SOC will drop.[52] Thus, the earlier the triplet-to-quintet crossover, the larger will be the SOC and the larger the p_{TQ} probability. This depends on the height of the $^5\mathbf{TS_H}$ species and its geometry. Inspection of Figure 9 shows that for the common RH molecule (**CH**), the earliest $^5\mathbf{TS_H}$ species occurs for the $\mathbf{K_{Bn-TPEN}}$ reagent. This analysis leads to the conclusion that the reactions of $\mathbf{K_{Bn-TPEN}}$ will be more prone than others to exhibit TSR in the scenario of **Case B**. Indeed, the reaction of $\mathbf{K_{Bn-TPEN}}$ with ethylbenzene exhibits $KIE_{H/D}$ values of 50, while the same reaction with $\mathbf{K_{N4Py}}$ had $KIE_{H/D}$ of 30.[16] The large KIEs indicate tunneling as may be envisioned for **Case B**, and the variability of the $KIE_{H/D}$ may reflect the interplay of the KIEs for the two reacting states. We note that the analogous iron−oxo species of the enzyme *TauD* also exhibits large $KIE_{H/D}$ values;[11] since here the ground state is $S = 2$, the large $KIE_{H/D}$ may reflect tunneling through the quintet barrier, but the involvement of another a spin state should also be considered.

5. Conclusion

The six synthetic non-heme iron−oxo reagents ($^{2S+1}\mathbf{K_L}$, in Scheme 1) addressed in this study possess a triplet ($S = 1$) ground state and a low-lying quintet ($S = 2$) excited state. The UB3LYP calculations show that the energy gaps between the two states are rather small, 1−10 kcal/mol, and depend on the ligand. A simple orbital scheme (Scheme 2) is used to rationalize trends in terms of the energy gap between the two d orbitals; δ (which is doubly filled in the triplet state) and σ^*_{xy} (which becomes singly occupied in the quintet state), and the exchange interactions between the unpaired d-electrons.

The hydroxylation mechanisms promoted by these non-heme reagents follow the normal rebound mechanism with an H-abstraction phase followed by radical rebound.[2,16] However, due to the proximity of the two spin states, the hydroxylation can proceed on the two surface and thereby exhibits two-state reactivity (TSR).[22,28,51] The triplet surface exhibits *a stepwise mechanism where the initially formed organic radical possesses a significant barrier for rebound*. By contrast, in most cases, the mechanism on the quintet surface is *effectively concerted*, since the rebound process is barrier free. The trends in the H-abstraction and rebound barriers, the structures of the corresponding transition states, and other features, can all be well understood using a simple orbital evolution scheme (Scheme 3) that shows the patterns of electronic reorganization in the various steps on the two surfaces.

Since the two spin-state surfaces are very close, the entire seam of crossing is in principle accessible for spin-state transitions, thereby suggesting that the observed reactivity patterns will reflect the interplay of triplet−quintet states. The possible TSR scenarios are suggested depending on the initial triplet−quintet gap (Scheme 6); when the gap is very small, one may anticipate an initial spin-state equilibrium followed

by reaction on the quintet surface (**Case A**), and when the gap is larger, spin-state transition will occur en route to ^{5}**TS$_H$**, the H-abstraction quintet transition state (**Case B**). In the latter case, the spin crossover and H-abstraction occur together, and both processes tunnel through the triplet barrier. An attempt is made to rationalize the experimental data along these lines.

The TSR model makes a few testable predictions: (a) If crossing to the quintet state (**Cases A** and **B**) occurs with a good probability, the hydroxylation will be effectively concerted, whereas if it transpires only on the triplet surface, one will expect side products similar to radical intermediates (e.g., loss of stereochemistry, scrambling, etc.). (b) In **Case B** one expects kinetic isotope effects (KIEs) typical of tunneling. (c) In intermediate situations, where the two surfaces contribute to the rate, one expects to see intermediate KIEs and radical scrambling patterns that arise from two processes. (d) Solvent effects in these non-heme reagents are expected to be very large.

Acknowledgment. S.S. acknowledges support by the German Federal Ministry of Education and Research (BMBF) within the framework of the German-Israeli Project Cooperation (DIP). This paper is dedicated to the memory of Prof. F. Bernardi.

Supporting Information Available: Eleven tables, 18 figures, and complete ref 32. This material is available free of charge via the Internet at http://pubs.acs.org.

JA061609O